

# Extracting Secret Keys from Integrated Circuits

by

Daihyun Lim

Submitted to the Department of Electrical Engineering and Computer  
Science

in partial fulfillment of the requirements for the degree of

Master of Science in Electrical Engineering and Computer Science

at the

MASSACHUSETTS INSTITUTE OF TECHNOLOGY

May 2004 [June 2004]

© Massachusetts Institute of Technology 2004. All rights reserved.

Author ..... /.....

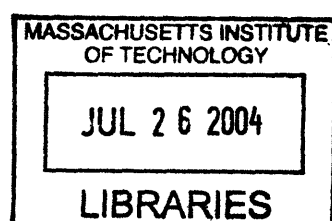
Department of Electrical Engineering and Computer Science  
May 20, 2004

Certified by ..... /.....

Srinivas Devadas  
Professor of Electrical Engineering and Computer Science  
Thesis Supervisor

Accepted by ..... /.....

Arthur C. Smith  
Chairman, Department Committee on Graduate Students ARCHIVES





# **Extracting Secret Keys from Integrated Circuits**

by

Daihyun Lim

Submitted to the Department of Electrical Engineering and Computer Science  
on May 20, 2004, in partial fulfillment of the  
requirements for the degree of  
Master of Science in Electrical Engineering and Computer Science

## **Abstract**

Modern cryptographic protocols are based on the premise that only authorized participants can obtain secret keys and access to information systems. However, various kinds of tampering methods have been devised to extract secret keys from widely fielded conditional access systems such as smartcards and ATMs. As a solution, Arbiter-based Physical Unclonable Functions (PUFs) are proposed. This technique exploits statistical delay variation of wires and transistors across integrated circuits (ICs) in the manufacturing processes to build a secret key unique to each IC. We fabricated Arbiter-based PUFs in custom silicon and investigated the identification capability, reliability, and security of this scheme. Experimental results and theoretical studies show that a sufficient amount of variation exists across ICs. This variation enables each IC to be identified securely and reliably over a practical range of environmental variations such as temperature and power supply voltage. Thus, arbiter-based PUFs are well-suited to build key-cards and membership cards that must be resistant to cloning attacks.

Thesis Supervisor: Srinivas Devadas  
Title: Professor of Electrical Engineering and Computer Science



## Acknowledgments

This work was funded by Acer Inc., Delta Electronics Inc., HP Corp., NTT Inc., Nokia Research Center, and Philips Research under the MIT Project Oxygen partnership.

First of all, I would like to extend my sincere gratitude to my advisor, Srinivas Devadas, for his inspiring advice and encouragement from the beginning through the end of this research. I have learned what research is and how fun it is from working with him. I also greatly thank Marten van Dijk, the guru of mathematics, who is always full of interesting ideas and ready to formulate and solve problems.

My gratitude also extends to all of Computation Structures Group people for their support and encouragement. I would like to specially thank Blaise Gassend, who answered many of my questions and provided me a Debian Linux environment, which has played an important role in PUF experiments. I also appreciate Jaewook Lee for his help in designing and fabricating test-chips for experiments in this thesis. Edward Gookwon Suh provided me a cute thermometer that made it possible to measure the temperature variation of PUFs. My old office-mate Prabhat Jain deserves special credit for his advices about how to survive here from the beginning of my MIT life. I warmly thank my current office-mate Charles O'Donnell, the excellent rower who is better than any other woman in the world, and Michael Zhang, the enthusiastic pool player who hates to lose every game, for their outstanding advices about writing.

I thank all of my friends who have made my life at MIT so enjoyable, especially my girl-friend Jerin Gu.

Last, I would like to thank my mom for her love and encouragement.



# Contents

<b>1</b>	<b>Introduction</b>	<b>17</b>
1.1	Secure Storage of Secret Keys . . . . .	17
1.2	Random Functions as Secret Key Storage . . . . .	18
1.3	Exploiting Process Variation in Silicon Manufacturing . . . . .	19
1.4	Organization . . . . .	19
<b>2</b>	<b>Physical Random Functions for Secret Key Storage</b>	<b>21</b>
2.1	Definition of Physical Random Functions . . . . .	21
2.1.1	Definition of One Way Functions . . . . .	21
2.1.2	Definition of Physical Random Functions . . . . .	22
2.2	Secret Key Storage . . . . .	23
2.2.1	Manufacturer Resistant PUFs . . . . .	23
2.2.2	Applications . . . . .	24
<b>3</b>	<b>Arbiter-Based PUF</b>	<b>27</b>
3.1	Delay-Based Authentication . . . . .	27
3.1.1	Statistical Delay Variation . . . . .	27
3.1.2	Measurement of Delays . . . . .	28
3.1.3	Generating Challenge-Response Pairs . . . . .	30
3.2	Arbiter-Based PUF . . . . .	30
3.2.1	General Description . . . . .	31
3.2.2	Switch Blocks and Delay Paths . . . . .	32
3.2.3	Arbiter . . . . .	33

3.3	Analysis and Characterization of Arbiter-Based PUF . . . . .	35
3.3.1	Inter-chip Variation . . . . .	35
3.3.2	Reliability . . . . .	38
3.3.3	Performance . . . . .	40
3.3.4	Aging . . . . .	40
<b>4</b>	<b>Modeling an Arbiter-Based PUF</b>	<b>43</b>
4.1	Delay Model . . . . .	44
4.1.1	Linear Delay Model . . . . .	44
4.1.2	Non-Linear Delay Model . . . . .	45
4.2	Estimation of Model Parameters . . . . .	46
4.2.1	Estimation of $s_i/\sigma$ . . . . .	46
4.2.2	Estimation of $\sigma_\Delta/\sigma_p$ . . . . .	48
4.2.3	Estimation of $\sigma_\Delta/\sigma_p$ using a Non-linear Delay Model . . . . .	53
4.3	Experiments . . . . .	55
4.3.1	Estimation of $s_i$ . . . . .	55
4.3.2	Estimation of $\sigma_\Delta/\sigma_p$ . . . . .	56
4.3.3	Estimation of Non-linearity . . . . .	57
4.4	Identification/Authentication Capability . . . . .	59
4.4.1	Inter-chip Variation and Environmental Variation . . . . .	59
4.4.2	Identification/Authentication Capability . . . . .	64
<b>5</b>	<b>Breaking an Arbiter-Based PUF</b>	<b>69</b>
5.1	Attack Models . . . . .	69
5.1.1	Duplication . . . . .	70
5.1.2	Timing-Accurate Model Building . . . . .	70
5.1.3	Software Model Building Attacks . . . . .	72
5.2	Software Modeling Building Attack: Support Vector Machines . . . . .	72
5.2.1	Additive Delay Model of a PUF Circuit . . . . .	73
5.2.2	Support Vector Machines . . . . .	75
5.3	Experiments . . . . .	77

5.3.1	Experiments using a FPGA implementation . . . . .	77
5.3.2	Experiments using a Custom Silicon Implementation . . . . .	78
<b>6</b>	<b>Strengthening an Arbiter-Based PUF</b>	<b>81</b>
6.1	Secure Delay Models . . . . .	82
6.1.1	Feed-forward Arbiter Approach . . . . .	82
6.1.2	Non-linear Arbiter-based PUF Approach . . . . .	91
6.2	Reliability . . . . .	94
6.2.1	Distribution of Random Challenges . . . . .	95
6.2.2	Robust Challenges . . . . .	96
<b>7</b>	<b>Conclusion</b>	<b>103</b>
7.1	Ongoing and Future Work . . . . .	103
7.1.1	Reliable Secret Sharing with PUFs . . . . .	103
7.1.2	Reconfigurable PUFs using Non-volatile Storage . . . . .	105
7.1.3	PUF-based Physical Random Number Generators . . . . .	106
<b>A</b>	<b>Parameter Estimation</b>	<b>109</b>
<b>B</b>	<b>Properties of <math>Q(x)</math></b>	<b>113</b>



# List of Figures

2-1	The general model of identification system based on a PUF key-card . . . . .	25
2-2	The model of PUF-based membership cards. . . . .	26
3-1	The direct delay measurement using a ring oscillator circuit . . . . .	28
3-2	The relative delay measurement using a comparator circuit . . . . .	29
3-3	The structure of an arbiter-based PUF (basic arbiter scheme). . . . .	31
3-4	Implementation of a switch component. . . . .	32
3-5	A simple transparent data latch primitive and its signal transitions . .	33
3-6	Compensating for the arbiter skew by fixing the most significant bits of a challenge vector. . . . .	34
3-7	The density function of the random variable $p = \text{Prob}(R(c) = 1)$ . . .	36
3-8	The density of the inter-chip variation $y_{i,j}$ for a number of PUF pairs.	38
3-9	The inter-chip variation of the PUFs from a single wafer and across wafers. . . . .	39
3-10	The variation of PUF responses subjected to temperature and supply voltage changes. . . . .	40
3-11	The aging effect on an arbiter-based PUF for 25 days. . . . .	41
4-1	Accuracy intervals and their overlapping region. . . . .	52
4-2	Estimated skew parameters and their accuracy intervals from indepen- dent experiments. . . . .	55
4-3	Estimated $\sigma_P$ and their accuracy intervals from independent experiments.	56
4-4	Comparison of $p_t$ - $R'_t$ curves depending on the existence of non-linear noise. . . . .	58

4-5	The change of $\eta$ according to the number of PUFs and $\sigma_P$ . . . . .	60
4-6	The change of $\tau$ according to the number of the stages in delay paths. . . . .	63
5-1	The notations of delay segments in each stage. . . . .	73
5-2	The bounding planes with a soft margin and the plane approximately separating classes . . . . .	76
5-3	The lookup table implementation of a multiplexer in Xilinx FPGAs [2].	77
5-4	The improvement of prediction error rate of the software model according to the size of a training set. . . . .	78
6-1	Adding unknown challenge bits using feed-forward arbiters (feed-forward arbiter scheme). . . . .	82
6-2	Comparison of inter-chip variation between regular arbiter PUFs and feed-forward arbiter PUFs . . . . .	83
6-3	Estimates of $\sigma_P$ and their accuracy intervals for feed-forward arbiter PUFs. . . . .	85
6-4	Temperature and power supply voltage variations of feed-forward arbiter PUFs. . . . .	86
6-5	The feed-forward arbiter circuit with one feed-forward stage. . . . .	87
6-6	The feed-forward arbiter circuit with two feed-forward stages. . . . .	89
6-7	A candidate of the non-linear delay paths with non-linear functions. . . . .	91
6-8	Inter-chip variation, temperature variation, and voltage variation of non-linear arbiter PUFs. . . . .	92
6-9	Comparison of non-linearity between non-linear arbiter PUFs and regular arbiter PUFs. . . . .	94
6-10	Distribution of random challenges according to $\Delta(c)$ . . . . .	96
6-11	Distribution of random challenges according to the distance from the decision hyperplane. . . . .	97
6-12	Experimental results of $MIN(d_1, d_2)$ at different temperature. . . . .	102
7-1	The circuit diagram of a reconfigurable arbiter-based PUF. . . . .	106

7-2 The density function of the random variable $k$ , where $k$ is the number of 1s out of 200 repetitive measurements. . . . .	107
--	-----



# List of Tables

3.1	The transition table of a transparent data latch with an inverted gate	33
4.1	Measurement noises in the different number of stages. . . . .	64
6.1	Improvement of reliability using the robust challenges in 15 repetitive measurements. . . . .	98
6.2	Improvement of reliability using the robust challenges in $\pm 1.5\%$ voltage variation. . . . .	99
6.3	Improvement of reliability using the robust challenges to repetitive measurements and voltage variation. . . . .	100



# Chapter 1

## Introduction

### 1.1 Secure Storage of Secret Keys

For many emerging applications that need exceptional security in identifying and authenticating users, such as intellectual property protection, Pay-TVs, and ATMs, system security is based on the protection of secret keys. Malicious users can impersonate authorized users when the secret key is uncovered. Thus, private information storage devices, such as smartcards, provide active logical controls for the protection of secret information against logical and physical tampering attacks.

However, recently developed physical tampering methods such as micro-probing, laser cutting, glitch attacks, and power analysis have made it possible to extract digitalized secret information and compromise widely fielded conditional access systems. For example, an adversary can remove a smartcard package and reconstruct the layout of the circuit using chemical and optical methods. He can even read out the information stored in non-volatile memories such as EEPROMs and NVRAMs [13].

Researchers have invented various protection mechanisms to prevent invasive physical attacks. For example, we can introduce additional metalization layers that form a sensor mesh above the actual circuit [13]. The sensor mesh technique has been used in some commercial smartcard CPUs, such as the ST16SF48A and in some battery-buffered SRAM security processors, such as the DS5002FPM and DS1954. Using a sensor mesh, any interruption and short-circuit can be monitored while power is

available, and a laser cutter or selective etching access to bus lines can be prevented. Though a tamper-sensing environment can cause difficulty for the adversary, the sensor mesh cannot prevent the extraction of hard-wired information in a circuit when the power is off. However, it can erase keys stored in non-volatile memory as soon as tampering is detected.

Instead of using vulnerable hard-wired secret keys, we can exploit alternative circuit parameters that are resistant to physical attacks on the premise that the parameters can be converted into digital secret keys. Electrical properties such as signal propagation delays, threshold voltages, and power consumption form good candidates thank to their intrinsic randomness. In this thesis, we show how to build secure storage of secret keys based on propagation delays in ICs.

## 1.2 Random Functions as Secret Key Storage

Recently, the randomness of functions has attracted much attention for its cryptographic uses. The notion of pseudo-random functions based on computational complexity is presented in [11]. The idea of using random functions as secure storage of secret keys is discussed in [10]. Though pseudo-random functions are cryptographically strong against logical attacks, physical implementations of random functions are still vulnerable to duplication of the secret keys by sophisticated reverse engineering.

Therefore, instead of computational complexity, using randomness in physical materials can give a viable solution. As an example, the concept of Physical One-Way Functions (POWFs) has been introduced in [18]. In this work, Pappu et. al. show that the mesoscopic physics of coherent transport through a disordered medium can be used to allocate and authenticate unique identifiers by physically reducing the medium's micro-structure to a fixed-length string of binary digits. This POWF can be used to build a random function that keeps a logical strength of a pseudo-random function [11]. These physical random functions are strong against physical attacks because an adversary is not in control of heterogeneous materials that hold secret information.

## 1.3 Exploiting Process Variation in Silicon Manufacturing

Silicon can be a good candidate of a base material to build physical random functions. Gassend et. al. have introduced silicon physical random functions (also called Physical Unclonable Functions or PUFs for short) [8]. A PUF is based on the intrinsic random process variation in the manufacturing of ICs. While ICs can be reliably mass-manufactured to have identical digital functionalities, each IC can also be uniquely characterized due to inherent manufacturing variation. Since the responses of the PUF are designed to be sensitive to delay variation, process variation of transistors and wires delays across ICs makes the response pattern of each PUF unique. Thus, we can identify and authenticate each IC reliably by observing the PUF responses.

Since process variation is largely beyond the manufacturers' control, it is impossible for an adversary to make identical copies of a PUF. Moreover, since the manufacturing variation is small compared to other measurable circuit parameters, characterizing PUFs by probing internal propagation delays is an arduous task.

In this work, we propose a novel architecture, an *arbiter-based PUF*. By utilizing a differential structure, this approach makes the PUFs more reliable against environmentally induced noise. We thoroughly investigate the identification capability, reliability and security of this approach in this thesis. We develop a theoretical model of delay variation to estimate the feasibility of this approach in the mass-production of ICs. PUF test-chips were fabricated using a TSMC 0.18  $\mu m$  process. Using the test-chips, we estimate the model parameters and verify the correctness of the theoretical model. We also study the reliability of an arbiter-based PUF approach. Lastly, we propose alternative architectures to improve the security of the arbiter-based PUFs.

## 1.4 Organization

This thesis is structured as follows. Chapter 2 defines physical random functions, describes manufacture resistance of PUFs, and gives a general overview of PUF sys-

tems.

Chapter 3 introduces the notion of delay-based authentication and a detailed circuit implementation of arbiter-based PUFs. Furthermore, we show experimental results for silicon PUFs implemented in custom silicon, and analyze the important characteristics of PUFs such as inter-chip variation, measurement noise and environmental noise. We also measure the performance and an aging effect in arbiter-based PUFs.

Chapter 4 details the statistical model of an arbiter-based PUF circuit. We provide an appropriate delay model of a PUF circuit and estimate model parameters. Based on the model, we examine theoretical identification capability of arbiter-based PUFs. We calculate the required number of measurements to identify billions of PUFs with negligible probability of error. Moreover, we propose a parameter estimation method to verify the accuracy of the model based on experimental results.

Chapter 5 studies the vulnerability of arbiter-based PUFs against possible attack models. We provide a representation of arbiter responses as a linear function of challenges and delay segments. Based on the linear model, we investigate a machine learning algorithm, a Support Vector Machine (SVM), which can be trained by a small amount of challenge-response pairs to predict responses of given random challenges. We conclude that a software model building approach is critical to the security of arbiter-based PUFs.

Chapter 6 suggests alternative types of arbiter-based PUFs for which it is more difficult to build a software model by adding non-linearity in delay paths. From our experiments, we evaluate each PUF’s identification capabilities and estimate the amount of non-linearity of the delay model using the method in Chapter 4. The increased amount of non-linearity creates difficulty in model building for the new arbiters.

Finally, Chapter 7 concludes the thesis and presents ideas for future work such as reconfigurable PUFs and a PUF-based random number generator. We also present a reliable secret sharing method using PUFs.

# Chapter 2

## Physical Random Functions for Secret Key Storage

Pseudo Random Functions (PRFs) have attracted attention in modern cryptography. Because of their intriguing properties such as *indexing*, *poly-time evaluation*, and *pseudo-randomness*, PRFs have been used in various cryptographic applications [10], in particular, user identification and authentication. Though PRFs are cryptographically strong, sophisticated physical attacks can still break the PRF circuit to extract sensitive data.

In this chapter, we define a Physical Unclonable Function (PUF), which is constructed based on the randomness of physical materials to prevent physical attacks while keeping the cryptographic strength of the PRFs. As applications, we present a secure key-card system and Unclonable membership card system that are based on the existence of PUFs.

### 2.1 Definition of Physical Random Functions

#### 2.1.1 Definition of One Way Functions

Modern cryptography is based on the gap between efficient encryption for legitimate users and the computational infeasibility of decryption. Thus, a cryptographic al-

gorithm requires available *primitives* with special kinds of computational hardness properties. A *one-way function* is a basic primitive in the modern cryptographic system. Informally, a function is one-way if it is easy to compute but hard to invert. By “easy”, we mean that the function can be computed using a probabilistic polynomial time (PPT) algorithm, and by “hard” that there is no PPT algorithm to invert it with greater than “negligible” probability.

Here is the formal definition of one-way functions.

**Definition 2.1.1.** A function  $f : \{0, 1\}^* \rightarrow \{0, 1\}^*$  is called *strongly one-way* if the following two conditions hold.

- *Easy to compute:* There exists a deterministic polynomial time algorithm  $A$  such that on input  $x$ ,  $A$  outputs  $f(x)$  (that is,  $A(x) = f(x)$ ).
- *Hard to invert:* For every probabilistic polynomial time algorithm  $A'$ , every polynomial  $P$ , and all sufficiently large  $n$

$$\Pr(A'(f(y)) \in f^{-1}(f(y))) < \frac{1}{p(n)}.$$

The second condition means that the probability that algorithm  $A'$  will find an inverse of  $y$  under  $f$  is negligible. The strong one-way functions above require that any efficient inverting algorithm has negligible success probability. Weak one-way functions require only that all efficient algorithms fail with some non-negligible probability.

If the size of the output, i.e.,  $f(x)$ , is always fixed, regardless of the size of the input  $x$ , then the function  $f(x)$  is called a *one-way hash function*. This definition of one-way hash function will be used as a template when we define physical random functions in the next section.

### 2.1.2 Definition of Physical Random Functions

We can construct a poly-random collection of functions that cannot be distinguished from pure random functions based on the existence of one-way functions [11]. Instead

of using computational complexity, we can exploit the physical randomness in nature, such as heterogeneous optical medium, electrical noise, and process variation in silicon manufacturing, to construct random functions.

Here, we provide a general definition of *physical random functions* based on the definition of one-way functions [8]. The term *challenge* refers to the input to the functions and *response* refers to the output.

**Definition 2.1.2.** A *Physical Random Function* is the function embodied by a physical device, and maps challenges to responses. A physical random function satisfies the following properties:

- *Easy to evaluate:* The physical device can easily evaluate the function in a short period.
- *Hard to predict:* From a polynomial number of plausible physical measurements (in particular, determination of chosen challenge-response pairs (CRPs)), an adversary who no longer has the device and can only use a polynomial amount of resources (time, matter, etc.) can extract only a negligible amount of information about the response to a randomly chosen challenge.

By the term “easy”, we mean that the function can be computed in polynomial time. The term “plausible” is relative to the current state of the art in measurement techniques and is likely to change as methods improve.

The definition of the physical random function is similar to that of one-way functions. However, unlike a one-way function, it does not need to be hard to invert. For a physical random function, guessing the response from a given challenge without using the device must be hard.

## 2.2 Secret Key Storage

### 2.2.1 Manufacturer Resistant PUFs

Here we define *Manufacturer Resistant PUFs*.

**Definition 2.2.1.** A type of PUF is said to be *Manufacturer Resistant* if it is technically infeasible to produce two identical copies given only a polynomial amount of resources (time, money, silicon, etc.) [8].

In this thesis, we use the physical parameter variation in manufacturing process such as propagation delays in ICs to implement manufacturer resistant PUFs. Since the process variation is beyond the control of manufacturers, the PUF circuit is hard to duplicate.

### 2.2.2 Applications

PUFs can be used in many kinds of applications that need exceptional security in storing secret keys. Here, we present a key-card and membership card applications. These applications are based on PUFs to prevent a cloning attack by an adversary.

#### PUF Key-Cards

PUFs can be used to realize authenticated identification, in which only someone who physically possesses a PUF can access to protected resources. Since the PUF cannot be duplicated even by its manufacturer, the privilege of possessing the PUF cannot be abused with thousands of illegal copies. Figure 2-1 shows a general model of an authenticated identification process with a PUF key-card [2].

In this model, a principal with a PUF key-card presents it to a terminal at a locked door. The terminal can connect via a private, authentic channel to a remote, trusted server. The server has an established list of CRPs of the PUF. When the principal presents the card to the terminal, the terminal contacts the server using the secure channel, and the server replies with the challenge of a randomly chosen CRP in its list. The terminal inputs the challenge to the PUF, which determines a response. The response is sent to the terminal and forwarded to the server via the secure channel. The server checks that the response matches its expectation, and sends an acknowledgment to the terminal. The terminal then unlocks the door, allowing the user to access the protected resource. The server should only use each

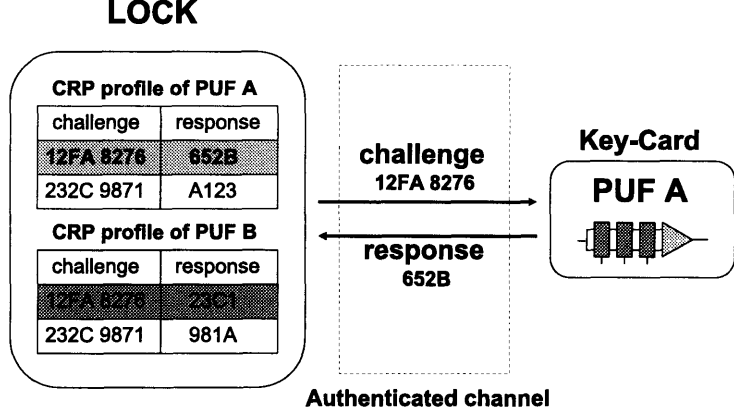


Figure 2-1: The general model of identification system based on a PUF key-card

challenge once to prevent replay attacks. Thus, the user is required to securely renew the list of CRPs on the server periodically.

### PUF-based Membership Cards

As an application of a pseudo random function, the “identifying friend or foe” problem has been suggested in [10]. This problem assumes an exclusive society that wants to give membership cards to all society members. These cards enable all society members to identify and authenticate each other. A president can exploit a pseudo-random function  $f_s$  for this use. For example, when Alice meets Bob, Alice gives a random input  $z$  to Bob, and Bob calculates  $f_s(z)$  and gives it back to Alice. Then Alice computes  $f_s(z)$  and compares it with the Bob’s result to authenticate Bob. In this scheme, if an adversary steals  $f_s$  and duplicates it using sophisticated physical attacks, the privileges of the society can be abused by a number of illegal copies.

Figure 2-2 shows a PUF-based membership card model as a solution against the duplication attack. A PUF membership card consists of a PUF and  $n - 1$  small CRP profiles of other users where  $n$  is the number of total users. The number of CRPs in each profile is sufficiently large to identify each PUF without an error.

The identification and authentication processes are similar. When Alice meets Bob, Alice asks Bob who he is, and Bob answers with his name. Then, Alice authen-

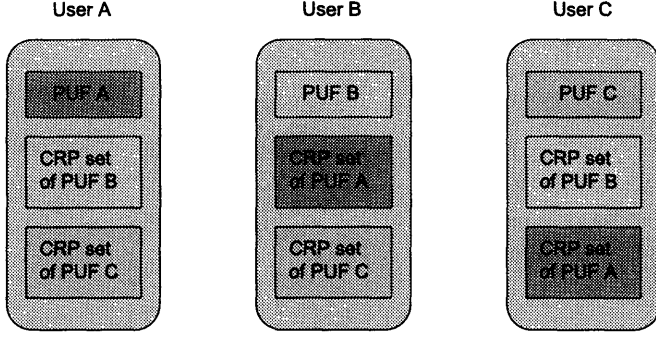


Figure 2-2: The model of PUF-based membership cards.

ticates Bob by evaluating Bob’s PUF and comparing the generated CRPs with Bob’s CRPs in her memory.

When the membership card is stolen by an adversary, he can read and duplicate CRP profiles of other users in the stolen card. However, he cannot make illegal copies of the card to impersonate the original user since he cannot duplicate the PUF in the card. Thus, only one non-member, who has the original card, is allowed to enjoy privileges of the society.

Though PUF-based membership cards can prevent the illegal duplication by an adversary, some problems must be considered. For example, if an adversary possesses multiple cards  $U_1$  and  $U_2$ , then he can extract the CRP profile of  $U_1$  from the database of  $U_2$ . Then, he can use this profile as a model to impersonate  $U_1$ . Moreover, the model can easily be duplicated since it is in a digital form. To prevent this attack, the CRP profiles of  $U_1$  in other users’ cards must be disjoint from each other. Additionally, all cards must be updated when adding a new user to the society. The overhead of the user addition confines an application of this scheme to an exclusive society where the addition of a new user occurs relatively infrequently. We can employ remote updating mechanisms as long as they are not expensive and do not cause security problems.

# Chapter 3

## Arbiter-Based PUF

To build a PUF in silicon, we must use circuit parameters that are beyond manufacturers' control. There are three requirements for a circuit parameter to be used as a primitive of PUFs: sufficient measurable variation across ICs, reliability against environmental variations, and difficulty in model building. The propagation delays of transistors and wires in ICs can satisfy these requirements. In this chapter, we investigate the characteristics of propagation delays as a PUF primitive. We propose an arbiter-based PUF scheme as an implementation of the delay variation measurement. We study the feasibility of this arbiter-based PUF scheme using experimental results.

Section 3.1 considers how to exploit inevitable process variation across dies, wafers, and lots, which changes propagation delays in the wires and transistors of ICs. In particular, we account for the advantages of a relative delay measurement method. In Section 3.2, we introduce an arbiter-based PUF and give its detailed structure. Section 3.3 provides experimental results and discusses the feasibility of this scheme.

### 3.1 Delay-Based Authentication

#### 3.1.1 Statistical Delay Variation

Process variation in the manufacturing of ICs must be considered to determine the performance and reliability of circuits. When a circuit is replicated across dies or

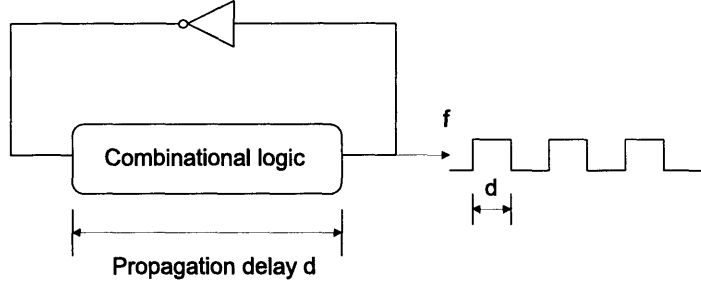


Figure 3-1: The direct delay measurement using a ring oscillator circuit

across wafers, process variation causes appreciable differences in the physical parameters of materials such as thickness, length, width and doping concentration. These variations result in the fluctuation of circuit parameters such as transistor channel length and threshold voltage, which determine propagation delays in ICs.

Across a die, device delays vary due to mask variations; this delay variation is called the system component of delay variation. There are also random variations in dies across a wafer and from wafer to wafer due to, for instance, process temperature and pressure variations during manufacturing steps. The magnitude of delay variation due to this random component can be over 5% for metal wires and is even higher for gates (cf. Chapter 12 of [5]). Delay variations of the same wire or device in different dies have been modeled using Gaussian distributions and other probabilistic distributions [3].

### 3.1.2 Measurement of Delays

#### Direct Delay Measurement

Propagation delays in ICs can be measured precisely using a ring oscillator [1]. In Figure 3-1, an oscillation period is proportional to the delay in a combinational circuit. Therefore, we can measure the delay by counting the number of rising edges of  $f$  for a fixed amount of time. The precision of delay measurement depends on the length of measuring time.

However, environmental variations such as temperature and supply voltage can

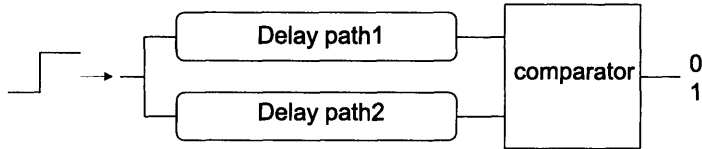


Figure 3-2: The relative delay measurement using a comparator circuit

cause critical reliability issues [20]. To improve the reliability of delay measurements under environmental variations, a compensated delay measurement has been studied in [2]. In the compensated delay measurement, instead of using an absolute delay value, we measure delays of two combinational circuits and take the ratio between two delay values as a response. Using this compensated delay measurement, we can keep the environmental variation sufficiently below inter-chip variation to allow reliable identification. However, to achieve a high accuracy in measuring delays using the ring oscillator, we need a significant amount of time to accumulate the oscillating ticks. This slow measurement can be the bottleneck in system performance.

### Relative Delay Measurement

Relative measurement can result in fast and robust delay measurement. Figure 3-2 shows the concept of relative delay measurement. In this scheme, we do not measure an actual delay directly but extract information from the comparison of two delays. Even if environmental variation changes the absolute values of two delays, the difference between the two delays is likely to be preserved; the output of relative measurement is resistant to environmental variation. Furthermore, a measurement takes only one cycle since we do not need to accumulate oscillating ticks to measure the actual delays. Of course, in relative delay measurement, the amount of information per measurement is reduced because we can gain only one bit of information by one comparison. We can increase the amount of the information by replicating the same circuit up to the desired number of bits, although the size of the circuit will grow proportionally.

### 3.1.3 Generating Challenge-Response Pairs

Assuming no environmental noise, a PUF is a deterministic function whose responses are sensitive to delay variation in an IC. To identify individual ICs, we generate challenge-response pairs (CRPs) for each PUF, where the challenge can be a digital (or possibly analog) input stimulus, and the response depends on the transient behavior of the IC. A precisely measured delay and the delay ratio of two or more delays have been used as a PUF response in [8]. In this work, we use the digital output of a comparator called an *arbiter* as the PUF response.

We build a network of logic devices. The configuration of this network is determined by the challenge vector  $\mathbf{c} = (c_1, c_2, \dots, c_m)$ . There are two symmetric delay paths that go through the network, and a comparator generates a one-bit response by comparing two delays. Since the response is decided deterministically by a given challenge, there are  $2^m$  possible CRPs for a PUF, where  $m$  is the length of a challenge vector.

Since the PUF is designed to be highly sensitive to the process variation of delays in ICs, the responses of the same challenge across ICs can be different from each other. We define the inter-chip variation  $\tau$  between two different PUFs as

$$\tau = \text{Prob}(R_i(c) \neq R_j(c)),$$

where  $R_i(c)$  is the response of the  $i^{\text{th}}$  IC on a random challenge  $c$ , and  $i \neq j$ . By generating a sufficient number of CRPs, we can identify each IC with a negligible probability of error.

## 3.2 Arbiter-Based PUF

In this section, we describe an *arbiter-based PUF*, which utilizes relative delay measurement to generate CRPs.

### 3.2.1 General Description

In general, an arbiter-based PUF is composed of delay paths and an arbiter at the end of the delay paths. Figure 3-3 depicts the structure of an arbiter-based PUF. In this scheme, we excite two delay paths simultaneously and make the transitions race against each other. Then the arbiter at the end of the delay paths determines which rising edge arrives first and sets its output to 0 or 1 depending on a winner. This circuit takes an  $n$ -bit challenge ( $b_i$ ) as an input to configure the delay paths and generates a one-bit response as an output.

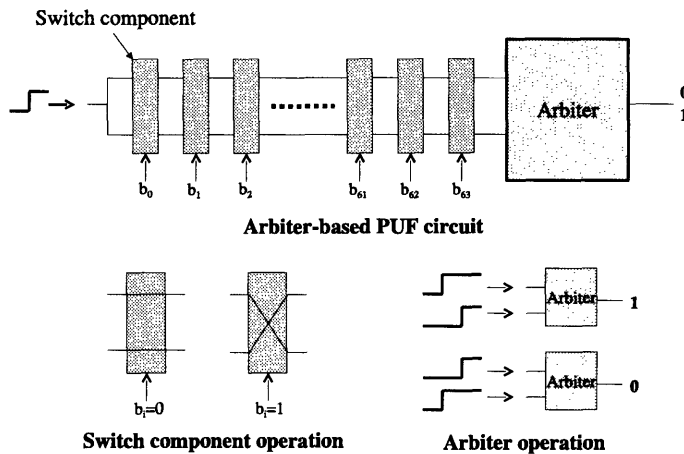


Figure 3-3: The structure of an arbiter-based PUF (basic arbiter scheme).

There are  $m$  switches and each of them can change the configuration of delay paths. Thus, the number of possible configurations of delay paths is  $2^m$ . At the end of the circuit, the delay difference between top and bottom paths is determined by the configuration of delay paths, and we denote the difference by  $\Delta(c)$ . The arbiter outputs 0 if  $\Delta(c)$  is greater than or equal to zero. Otherwise, it outputs 1.

Process variation changes  $\Delta(c)$  across ICs. When the amount of variation is greater than  $|\Delta(c)|$ , the response of an arbiter can be changed. Therefore, the challenges whose  $|\Delta(c)|$ 's are less than maximum process variation can give inter-chip variation in PUF responses. For the challenges whose  $|\Delta(c)|$  is greater than the max-

imum process variation, responses are biased to 0 or 1 and do not change across ICs. In order to maximize the inter-chip variation, the delay paths must be placed and routed as symmetrically as possible so as to minimize  $|\Delta(c)|$ .

### 3.2.2 Switch Blocks and Delay Paths

Figure 3-4 details the switch component of delay paths. This switch connects its two input ports ( $i_0$  and  $i_1$ ) to the output ports ( $o_0$  and  $o_1$ ) with different configurations depending on the control bit ( $b_i$ ); for  $b_i=0$  the paths go straight through, while for  $b_i=1$  they are crossed. It is simply implemented with a pair of 2-to-1 multiplexers and buffers.

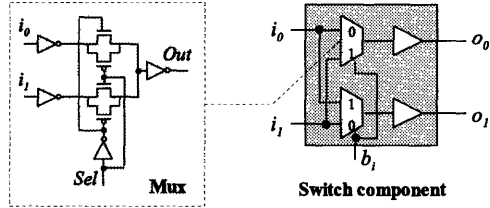


Figure 3-4: Implementation of a switch component.

In our test-chips, we symmetrically place and route the cells and cover the entire chip effectively using the wires in a delay circuit. This layout technique makes it extremely difficult for an adversary to probe internal nodes to read out a logic value without breaking the PUF, i.e., without changing the delays of wires or transistors.

If racing paths are symmetric in the layout regardless of the challenge bits and an arbiter is not biased to either path, a response is equally likely to be 0 or 1. The response is determined only by the delay variation in the manufacturing of ICs. Consequently, we wish to make delay paths as symmetric as possible to give a PUF sufficient inter-chip variation.

### 3.2.3 Arbiter

For an arbiter, we use a simple transparent data latch with an inverted gate. Figure 3-5 shows the latch primitive (LD\_1) of Xilinx FPGAs used as an arbiter and the signal transition diagram of the latch. In addition, Table 3.1 shows the detailed transitions of the LD\_1. If the rising edge of a data input  $D$  comes earlier than a rising edge of a gate input  $G$ , an output  $Q$  samples 1. Otherwise,  $Q$  becomes 0.

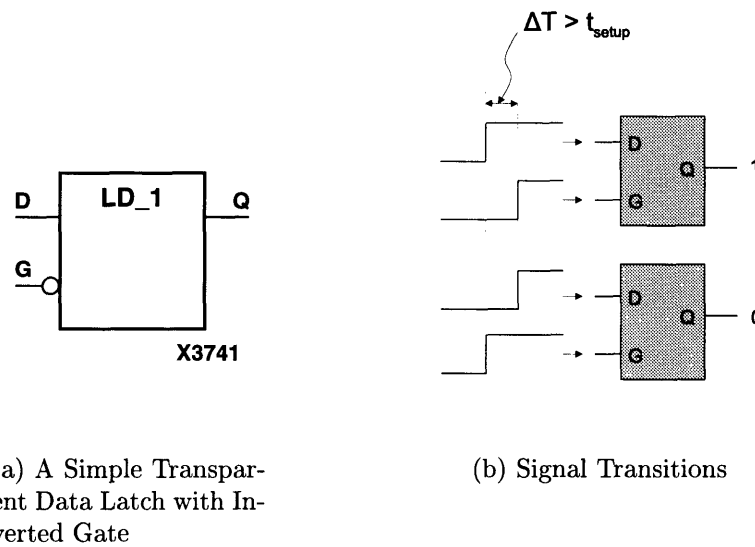


Figure 3-5: A simple transparent data latch primitive and its signal transitions

Inputs		Outputs
G	D	Q
0	0	0
0	1	1
1	X	No Change
↑	D	d

Table 3.1: The transition table of a transparent data latch with an inverted gate

In custom implementation of an arbiter, we note that since an output is preset to 0, and input signals must satisfy the setup time of a latch to switch the output to 1, this arbiter favors the path to output 0. More precisely, when the rising edge

of  $D$  comes earlier than that of  $G$ , an ideal arbiter output must be 1. However, if the time difference between two signals is less than the setup time of the latch, an output remains at 0 instead of being switched to 1. This property introduces a skew factor to a delay model of arbiter-based PUFs. We discuss the influence of this skew factor to inter-chip variation in Chapter 4. As a result of this skew, only 10% of total responses are 1s on average. This imbalance of PUF responses significantly reduces the identification capability of PUFs.

We can compensate for the skews by fixing several challenge bits to effectively lengthen the delay path connected to a gate input. Figure 3-6 shows how the compensation works. Since  $\text{Prob}(b_n = 0) = \text{Prob}(b_n = 1) = \frac{1}{2}$ , an effective skew in front of the  $n^{\text{th}}$  stage is  $s - \frac{\Delta_1 + \Delta_2}{2}$ , where  $s > 0$  is the skew of arbiter. When  $\Delta_1 > \Delta_2$ , we fix  $b_n$  at 0, and otherwise, we fix it to 1. After fixing the  $n^{\text{th}}$  bit, the effective skew becomes  $s - \text{Max}(\Delta_1, \Delta_2)$ , which is smaller than the original effective skew. In order to determine whether  $\Delta_1 > \Delta_2$  or not, a PUF is tested by 200 CRPs when  $b_n = 0$ , and  $b_n = 1$ . If the number of 1s when  $b_n = 0$  is greater than when  $b_n = 1$ ,  $b_n$  must be fixed to 0. Otherwise, we fix  $b_n$  to 1. Recursively, we fix the next most significant bit until  $\text{Prob}(R(c) = 1)$  approaches  $\frac{1}{2}$ . From experiments, we need to fix 12 of challenge bits to achieve roughly 50% 0's and 1's in responses. After this compensation, the size of a challenge vector space is reduced from  $2^{64}$  to  $2^{52}$ .

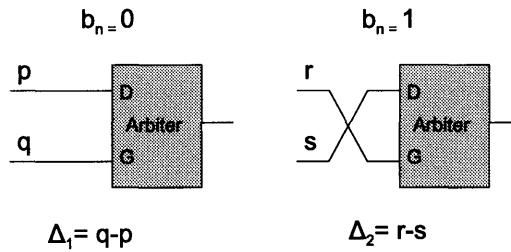


Figure 3-6: Compensating for the arbiter skew by fixing the most significant bits of a challenge vector.

### 3.3 Analysis and Characterization of Arbiter-Based PUF

In this section, we present the primary characteristics of arbiter-based PUFs such as *inter-chip variation*, *measurement noise*, and *environmental variations*, which decide the viability of this scheme.

Inter-chip variation is the measure of a distance between CRPs from two different PUFs. To identify each PUF from the billions of others, there must be a considerable amount of inter-chip variation between PUFs. In Section 3.3.1, we show experimental results of inter-chip variation between different PUFs.

Since a PUF uses an analog delay characteristic of an IC, PUF responses can be sensitive to environmental changes such as temperature and power supply voltage variation. Section 3.3.2 examines the causes of unreliability, such as measurement noise, environmental variation, and an aging effect. We show the experimental results of measurement noise and environmental variation over a practical range. In addition, we examine an aging effect that can potentially degrade identification capability after prolonged use.

#### 3.3.1 Inter-chip Variation

##### Information-Bearing Challenges

Let *information-bearing challenges* be the challenges whose responses in a number of different PUFs are not equal. We need a considerable number of information-bearing challenges to identify each PUF. To examine the existence of information-bearing challenges, we have measured responses for 10,000 challenges using 37 test-chips. For each challenge, we have calculated the probability of a response being 1 as follows.

$$p = \Pr(R(c) = 1) = \frac{k}{37},$$

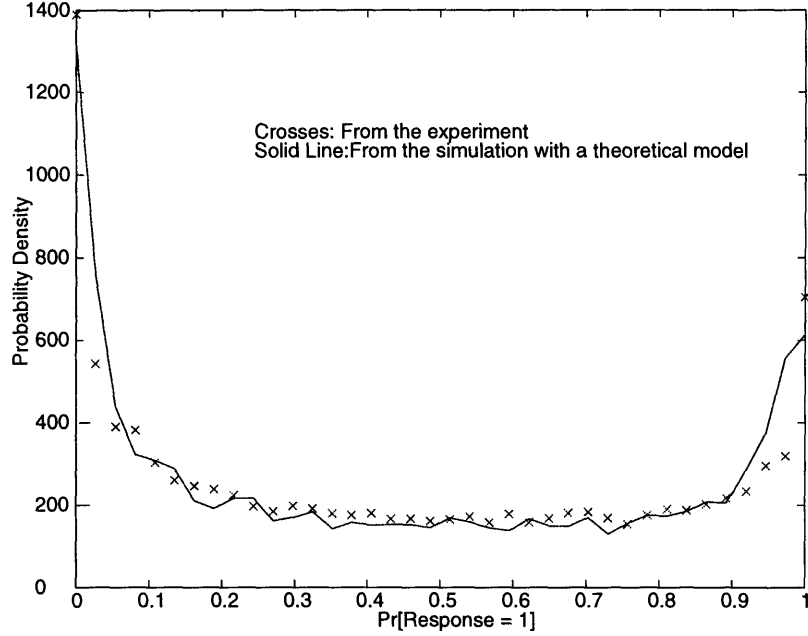


Figure 3-7: The density function of the random variable  $p = \text{Prob}(R(c) = 1)$

where  $k$  is the number of PUFs that output 1. Figure 3-7 shows the density function of the random variable  $p$  for 10,000 challenges. When  $p = 0$  or  $p = 1$ , the challenge does not generate any information since all PUF responses are equal. Except for the cases when  $p = 0$  or 1, more than 80% of the total challenges are information-bearing challenges.

We assume that process variation and the distribution of  $\Delta(c)$ , the delay difference between the top and bottom paths, are Gaussian (cf. Chapter 4). Let  $\sigma_p$  and  $\sigma_\Delta$  be the standard deviations of process variation and  $\Delta(c)$ , respectively. This probabilistic model can be simulated using MATLAB. In Figure 3-7, we have evaluated the model parameter  $\sigma_P = \frac{\sigma_\Delta}{\sigma_p}$  by fitting the simulation results into the experimental results. The evaluated  $\sigma_P$  is around 1.5. It is significantly smaller than  $\sigma_P \approx 25$  from the FPGA experiments in [2]. This difference comes from the asymmetry of delay paths in FPGAs, which increase  $\sigma_\Delta$  significantly.

## Definition and evaluation of inter-chip variation

**Definition 3.3.1.** Here, we define the inter-chip variation between two different PUFs as below. For two different PUF responses  $R_i(c)$  and  $R_j(c)$  to a challenge  $c$ , let

$$D_{i,j}(c) = \begin{cases} 1 & R_i(c) \neq R_j(c) \\ 0 & R_i(c) = R_j(c) \end{cases}.$$

For a random challenge set  $C$ , we define the inter-chip variation  $y_{i,j}$  between PUF  $i$  and  $j$  as

$$y_{i,j} = \frac{1}{|C|} \sum_{c \in C} D_{i,j}(c).$$

For convenience, we denote the inter-chip variation by  $(100 \cdot y_{i,j})\%$ .

We have evaluated  $y_{i,j}$ 's from 190 arbiter-based PUF pairs using a random challenge set  $C$ , where  $|C| = 100,000$ . In order to improve the reliability, the majority of 11 repeated measurements has been used as a response. Figure 3-8 shows the density function of 190 evaluated inter-chip variations. Our test-chips have 23% inter-chip variation on average, and the minimum inter-chip variation is 17%.

Assuming that all measurements of  $D_{i,j}(c)$  are independent of each other, the distribution of  $y_{i,j}$  can be approximated to Gaussian when  $|C|$  is large. Generally speaking, the shape of Figure 3-8 follows our Gaussian assumption. We present the detailed model of inter-chip variation in Chapter 4.

## Inter-chip variation across wafers

Since manufacturing variation consists of die-to-die, wafer-to-wafer, and lot-to-lot variations, inter-chip variation can possibly be dependent on die and wafer locations. To guarantee that there is sufficient inter-chip variation between the PUFs from the same wafer, we must examine the inter-chip variation within a single wafer and across wafers.

In this experiment, we use two sets of PUFs. One set corresponds to the PUFs manufactured from wafer 5 in our TSMC run, and the other is from wafer 6. We

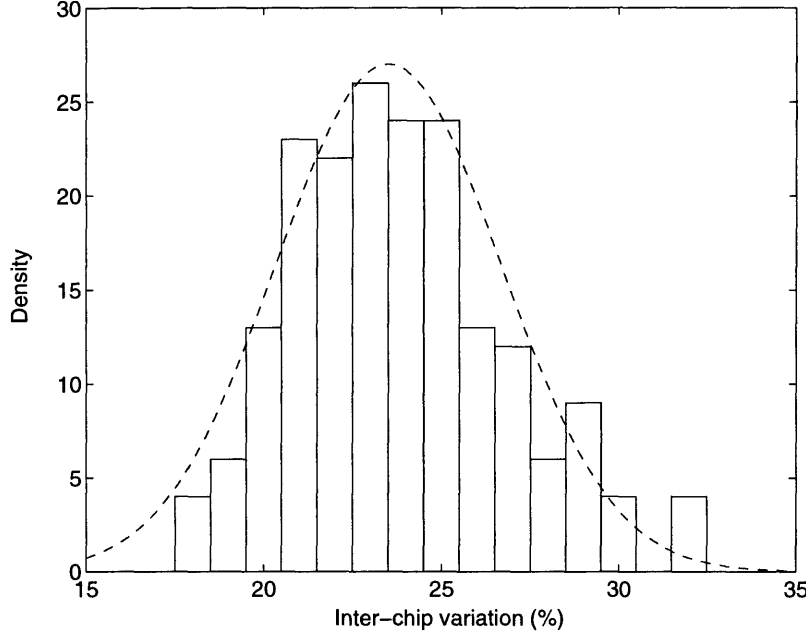


Figure 3-8: The density of the inter-chip variation  $y_{i,j}$  for a number of PUF pairs.

evaluate the average, minimum, and maximum inter-chip variation within wafer 5 or 6, and across the two wafers. Figure 3-9 shows the experimental results of inter-chip variation. The inter-chip variation across wafers is similar to the inter-chip variation from a single wafer. We conclude that there is a sufficient amount of inter-chip variation within a single wafer to identify each PUF from the wafer.

### 3.3.2 Reliability

Since a PUF is supposed to be a deterministic function, the response of the PUF must be consistent in repeated measurements. Unfortunately, environmental variations, instabilities in the circuit, and aging may cause unreliability in measured PUF responses. To quantify the effect of these variations, we define the *noise* ( $\mu$ ) as the probability that a newly measured response is different from the corresponding reference response.

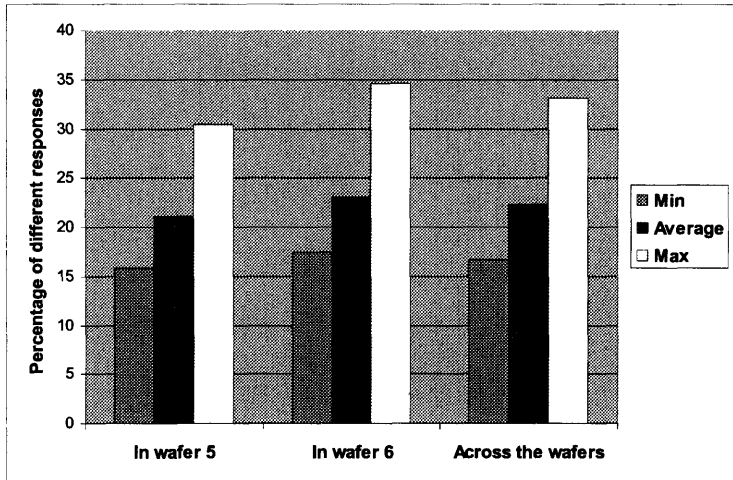


Figure 3-9: The inter-chip variation of the PUFs from a single wafer and across wafers.

### Measurement noise

A PUF response may change due to variations within a circuit even without environmental variation, which is called measurement noise ( $\mu_m$ ). For some challenges, a setup time violation for an arbiter may lead to an unreliable response. Furthermore, junction temperatures or internal voltages may slightly fluctuate as the circuit operates. This fluctuation can change the delay characteristics of PUFs. In the reference environment, we have estimated  $\mu_m \approx 0.7\%$ .

### Environmental variations

Temperature or power supply voltage variations can significantly change circuit delays and lead to unreliable responses. Since we exploit relative delay measurement, arbiter-based PUFs are robust to such environmental variations. Figure 3-10 shows the amount of environmental variation introduced by temperature ( $\mu_t$ ) and voltage variations ( $\mu_v$ ). The reference responses are measured at 27 °C and 1.8V power supply voltage. In this experiment, 10,000 challenges are used to estimate environ-

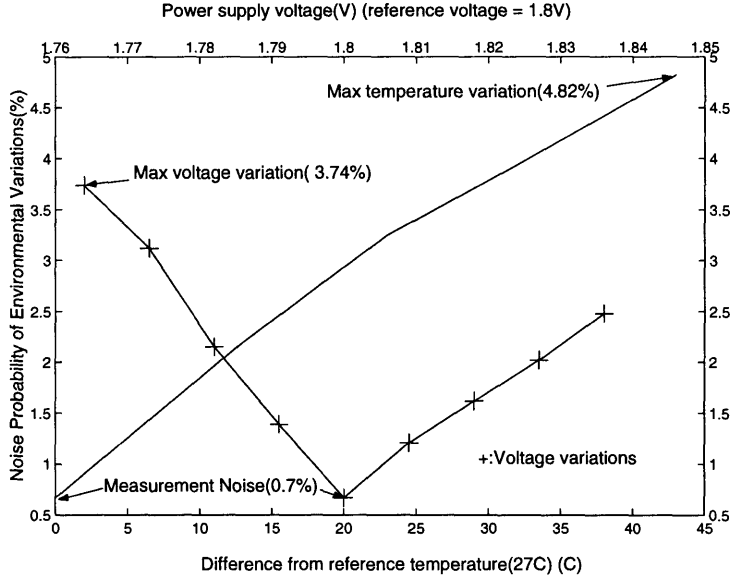


Figure 3-10: The variation of PUF responses subjected to temperature and supply voltage changes.

mental variations. Even if the temperature increases more than 40 degrees to 70 °C,  $\mu_t \approx 4.82\%$ . Also, with  $\pm 2\%$  power supply voltage variation,  $\mu_v \approx 3.74\%$ . Both  $\mu_t$  and  $\mu_v$  are well below the inter-chip variation of 23%.

### 3.3.3 Performance

For a given 64-bit challenge, it takes 50 ns for an input rising edge to transmit across the 64-stage parameterized delay circuit and evaluate an output at the arbiter. Therefore, if we want to generate 450 CRPs to distinguish billions of arbiter-based PUFs (cf. Section 4.4), it takes about 22.5  $\mu s$ . This is sufficiently fast for most applications since a PUF is evaluated only infrequently to obtain a secret. We can also boost the performance by replicating multiple delay paths and arbiters to evaluate the responses in parallel.

### 3.3.4 Aging

Electro-migration and hot-carrier effects cause the long-term degradation of the reliability of wires and transistors in an IC [4]. Since the behavior of a PUF relies on its

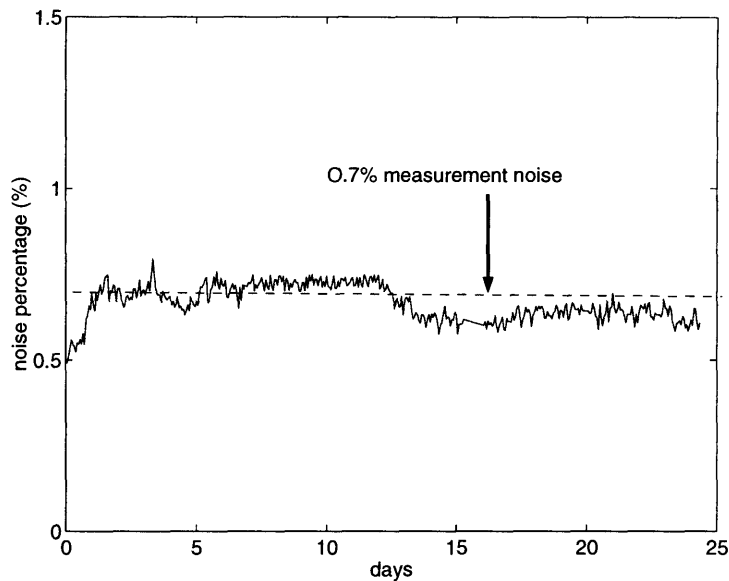


Figure 3-11: The aging effect on an arbiter-based PUF for 25 days.

transient response, we assume that the aging could seriously affect the security and reliability of a PUF. If the change due to aging is significant, we may not be able to recognize a PUF after the PUF has undergone long-term usage.

While we believe that the effect of aging is not a major problem compared to environmental variation, we have run a long-term aging experiment. Figure 3-11 shows the results of an aging test for one month. In the beginning of the test, we generated 100,000 CRPs as reference CRPs. During the test, we calculate the distance from new CRPs to the reference CRPs. The figure shows variation in the distance. Since the distance has not been notably increased over the 0.7% measurement noise, we conclude that there is no significant aging effect for a one-month test in a normal operating environment. In future work, the test must be performed in extreme environments such as high temperature and significant fluctuation of supply voltage.



# Chapter 4

## Modeling an Arbiter-Based PUF

In this chapter, we introduce the delay model of an arbiter-based PUF. We have already verified the feasibility of arbiter-based PUFs using 37 test-chips in Chapter 3. To prove that each PUF can be identified from billions of replicates, we introduce the probabilistic delay variation model. We estimate the parameters of the model using experimental results. Using the estimated parameters, we prove the identification capability of arbiter-based PUFs.

We propose a general parameter estimation method. When a model parameter  $z$  cannot be directly estimated but can be represented as a function of other estimable parameters, we can calculate the estimate  $\hat{z}$  from the estimates of other parameters. Using the general method, we can calculate the accuracy interval of the estimate  $\hat{z}$  and the error probability of the accuracy interval from the estimates of other parameters and their accuracy intervals.

We can verify the correctness of the delay model from an accuracy interval analysis. If experimental results do not follow the model, then we introduce a non-linear factor into the model and measure an amount of non-linearity in the experimental results. This measured non-linearity can be exploited as the metric of modeling complexity to examine the difficulty of model building in Chapter 6.

Section 4.1 presents a delay model of arbiter-based PUFs. Based on the model, Section 4.2 gives expressions of primary model parameters. These expressions are used to estimate the parameters as well as accuracy intervals of the parameters from

experimental results. Section 4.3 shows the experimental results of parameter estimation and verifies the correctness of our model with the presented theory. Section 4.4 proves the identification capability of arbiter-based PUFs based on inter-chip variation and maximum environmental variation from experimental results.

## 4.1 Delay Model

For deep sub-micron technologies, a combination of device physics, die location dependence, optical proximity effect, micro-loading in etching, and deposition may lead to heterogeneous and non-monotonic relationships among the process parameters. For the circuit that consists of continuous and differentiable functions, statistical delay variation can be approximated to a linear function of process conditions [16]. Therefore, without detailed understanding of the individual contributions of process conditions, we may assume that the propagation delay variation is Gaussian.

### 4.1.1 Linear Delay Model

In the description of our model, arbiter-based PUFs are numbered from 1 to  $n$ . We denote a challenge as  $c$ . Let  $R_i(c)$  be the response of a challenge  $c$  measured in the  $i^{\text{th}}$  PUF. In arbiter-based PUFs,  $R_i(c)$  is decided by a sign of a delay difference between top and bottom paths at the end of the delay paths. We denote the delay difference as  $\Delta_i(c)$ . In Section 3.2.3, we described the arbiter implementation using simple latches and the asymmetric behavior of the arbiter by a setup time constraint of an actual latch. This asymmetry introduces a skew in our delay model. We denote the skew of an arbiter in the  $i^{\text{th}}$  PUF by  $s_i$ . With  $\Delta_i(c)$  and  $s_i$ , we model  $R_i(c)$  as follows.

$$R_i(c) = \begin{cases} 1, & \text{if } s_i + \Delta_i(c) \leq 0, \\ 0, & \text{if } s_i + \Delta_i(c) > 0. \end{cases}$$

In our model, we decompose  $\Delta_i(c)$  into  $\Delta(c)$  and  $p_i(c)$ ,

$$\Delta_i(c) = \Delta(c) + p_i(c), \quad (4.1)$$

where  $\Delta(c)$  is a delay difference without process variation and  $p_i(c)$  is a process variation factor for a given challenge  $c$ . We can represent  $\Delta(c)$  as

$$\Delta(c) = \langle \mathbf{d}, \mathbf{c} \rangle,$$

where  $\mathbf{d} = (d_0, d_1, \dots, d_m)$  is a constant vector and  $\mathbf{c} = (c_0, c_1, \dots, c_m)$ ,  $c_i \in \{-1, 1\}$  is a random challenge vector (cf. Section 5.2.1). When  $m$  is sufficiently large, the distribution of  $\Delta(c)$  can be approximated to Gaussian by the Central Limit Theorem. Since each  $v_i$  has a zero mean,

$$\Delta(c) \sim N(0, \sigma_\Delta),$$

where  $\sigma_\Delta = \|\mathbf{d}\|$ . We assume the process variation  $p_i(c)$  to be Gaussian,

$$p_i(c) \sim N(0, \sigma_p).$$

Hence,

$$\Delta_i(c) \sim N(0, \sigma),$$

where  $\sigma = \sqrt{\sigma_\Delta^2 + \sigma_p^2}$ . In this model,  $\Delta(c)$  and  $p_i(c)$  are assumed to be independent of each other.

### 4.1.2 Non-Linear Delay Model

Ideally, statistical behavior of PUF responses must follow the linear delay model (cf. Section 5.2.1). However, in real circuits, various kinds of noise such as measurement noise, cross-coupling between wires, and environmental variations cause the delay model to be non-linear. In order to consider these non-linear effects, we extend the original model to

$$\Delta_i(c) = \Delta(c) + p_i(c) + \gamma, \quad (4.2)$$

where  $\gamma$  is a non-linearity factor. We assume that  $\gamma$  is from an arbitrary distribution and

$$|\gamma| \leq R, \quad (4.3)$$

where  $R$  is the upper-bound of non-linearity.

To measure the non-linearity of experimental results, first, we estimate a model parameter based on a linear delay model. If experimental results follow the linear model, the model parameter must be estimated consistently within a high probability accuracy interval in repeated independent experiments. Otherwise, we must introduce non-linearity  $\gamma > 0$  to give an extra margin to the accuracy interval. We increase the upper-bound  $R$  of non-linearity until all the estimates are included in the enlarged accuracy interval. This upper-bound  $R$  represents the amount of non-linearity in the experimental results.

## 4.2 Estimation of Model Parameters

In Section 4.2.1, we show how to estimate individual skews  $s_i$ 's using a linear delay model. In Section 4.2.2, we estimate  $\sigma_P = \sigma_\Delta/\sigma_p$  based on the estimated skews. In both sections, we derive the accuracy interval of an estimate and evaluate the probability that a model parameter exists in the accuracy interval. We show how to verify the correctness of model from accuracy intervals of estimates in repeated independent experiments. In Section 4.2.3, we estimate  $\sigma_P$  using the extended model with a non-linearity factor and derive an accuracy interval from the extended model.

### 4.2.1 Estimation of $s_i/\sigma$

In this section, a PUF  $i$  is fixed. Since

$$s_i + \Delta_i(c) \sim N(s_i, \sigma),$$

we obtain

$$\rho_i = \text{Prob}(R_i(c) = 1) = \text{Prob}\left(\frac{\Delta_i(c)}{\sigma} \leq -\frac{s_i}{\sigma}\right) = \int_{t=-\infty}^{-s_i/\sigma} \frac{e^{-t^2/2}}{\sqrt{2\pi}} dt = Q(-s_i/\sigma)$$

where

$$Q(x) = \int_{-\infty}^x \frac{e^{-t^2/2}}{\sqrt{2\pi}} dt.$$

Let  $C$  be a random challenge set. From the response set of  $C$ , we define  $y_i$  such that

$$y_i = \frac{1}{|C|} \sum_{c \in C} R_i(c). \quad (4.4)$$

By the law of large numbers, the binomial distribution which defines  $y_i$  tends to

$$y_i \sim N(\rho_i, \sqrt{\rho_i(1 - \rho_i)/|C|})$$

(notice that  $\rho_i(1 - \rho_i) \leq 1/4$ ). This proves that, when  $|C|$  is sufficiently large,

$$\begin{aligned} \text{Prob}(|y_i - \rho_i| \geq \varepsilon) &= 2Q(-\varepsilon/\sqrt{\rho_i(1 - \rho_i)/|C|}) \\ &\leq 2Q(-2\varepsilon\sqrt{|C|}) \end{aligned} \quad (4.5)$$

(see the inequality (B.1) in Appendix B). From the inequality (B.4) in Appendix B we obtain

$$\text{Prob}(|Q^{-1}(y_i) - Q^{-1}(\rho_i)| \geq \delta) \leq \text{Prob}(|y_i - \rho_i| \geq \varepsilon), \quad (4.6)$$

where<sup>1</sup>

$$\delta = \sqrt{2\pi}\varepsilon e^{Q^{-1}(y_i \pm \varepsilon)^2/2}. \quad (4.7)$$

From the inequalities (4.5) and (4.6), we can prove that  $\text{Prob}(|y_i - \rho_i| \geq \varepsilon)$  has the upper bound  $2Q(-2\varepsilon\sqrt{|C|})$ .

---

<sup>1</sup>We define  $f(y \pm \varepsilon) = \max\{f(y - \varepsilon), f(y + \varepsilon)\}$ .

Given  $|C|$  measurements, we choose  $\varepsilon$  as large as possible such that the bound  $2Q(-2\varepsilon\sqrt{|C|})$  is sufficiently small, say  $p_s$ . We compute  $\delta$  from Eqn. (4.7) and then, with an error probability less than  $p$ , the skew  $-s_i/\sigma$ , that is equal to  $Q^{-1}(\rho_i)$ , exists within the accuracy interval  $[Q^{-1}(y_i) - \delta, Q^{-1}(y_i) + \delta]$ .

#### 4.2.2 Estimation of $\sigma_\Delta/\sigma_p$

In this section, we use PUF  $i$  and PUF  $j$  ( $i \neq j$ ) to evaluate the probability that both PUFs output the same response 1. From our model, the process variation  $p_i(c)$  is from the normal distribution  $N(0, \sigma_p)$ . Let

$$\sigma_P = \sigma_\Delta/\sigma_p$$

be the ratio between the standard deviation of  $\Delta(c)$  and the standard deviation of process variation. We can derive  $Prob(R_j(c) = 1, R_i(c) = 1)$  using the parameters  $-s_i/\sigma$ ,  $-s_j/\sigma$ , and  $\sigma_P$ .

$$\begin{aligned} \rho_{i,j} &= Prob(R_j(c) = 1, R_i(c) = 1) \\ &= Prob(s_j + \Delta(c) + p_j(c) \leq 0, s_i + \Delta(c) + p_i(c) \leq 0) \\ &= Prob\left(\frac{p_j(c)}{\sigma_p} \leq -\frac{s_j}{\sigma} \sqrt{1 + \sigma_P^2} - \frac{\Delta(c)}{\sigma_\Delta} \sigma_P, \frac{p_i(c)}{\sigma_p} \leq -\frac{s_i}{\sigma} \sqrt{1 + \sigma_P^2} - \frac{\Delta(c)}{\sigma_\Delta} \sigma_P\right) \\ &= \int_{t=-\infty}^{\infty} \frac{e^{-t^2/2}}{\sqrt{2\pi}} Q(-(s_j/\sigma) \sqrt{1 + \sigma_P^2} - t\sigma_P) Q(-(s_i/\sigma) \sqrt{1 + \sigma_P^2} - t\sigma_P) dt \\ &= P(-s_i/\sigma, -s_j/\sigma, \sigma_P), \end{aligned}$$

where

$$P(v, w, z) = \int_{t=-\infty}^{\infty} \frac{e^{-t^2/2}}{\sqrt{2\pi}} Q(v\sqrt{1+z^2} - tz) Q(w\sqrt{1+z^2} - tz) dt$$

is a continuous differentiable function of three variables. For fixed  $i$  and  $j$ ,  $v = -s_i/\sigma$  and  $w = -s_j/\sigma$  are fixed. Intuitively,  $P(v, w, z)$  is a monotonically increasing function in  $z$  since a larger  $z = \sigma_P$  means less process variation and two responses are more

likely to be equal if there is less process variation. Thus, we can use a simple binary search to evaluate

$$z = P^\leftarrow(v, w, \theta) \quad (4.8)$$

as a solution of the equation  $\theta = P(v, w, z)$ .

Let

$$D_{i,j}(c) = \begin{cases} 1 & R_i(c) = 1, R_j(c) = 1 \\ 0 & \text{otherwise} \end{cases}$$

where  $i \neq j$ . For a random challenge set  $C$ , we define  $y_{i,j}$  as

$$y_{i,j} = \frac{1}{|C|} \sum_{c \in C} D_{i,j}(c). \quad (4.9)$$

Similarly, by the law of large numbers, the binomial distribution which defines  $y_{i,j}$  tends to

$$y_{i,j} \sim N(\rho_{i,j}, \sqrt{\rho_{i,j}(1 - \rho_{i,j})/|C|})$$

(notice that  $\rho_{i,j}(1 - \rho_{i,j}) \leq 1/4$ ). This proves that, when  $|C|$  is sufficiently large <sup>2</sup>,

$$\begin{aligned} \text{Prob}(|y_{i,j} - \rho_{i,j}| \geq \varepsilon) &= 2Q(-\varepsilon/\sqrt{\rho_{i,j}(1 - \rho_{i,j})/|C|}) \\ &\leq 2Q(-2\varepsilon\sqrt{|C|}) \end{aligned} \quad (4.10)$$

In Appendix A, we provide a general method to estimate a hidden parameter in a general model from the estimates of known parameters. If the hidden parameter can be represented as the function of directly estimable parameters, we can calculate the accuracy interval of the hidden parameter from the accuracy intervals of other parameters. The probability that the hidden model parameter exists in the accuracy interval can also be evaluated using the general method.

In our model,  $\sigma_P$  is the hidden parameter and it can be represented as a function of  $-s_i/\sigma$ ,  $-s_j/\sigma$ , and  $\rho_{i,j}$  in Eqn. (4.8). Since we can directly estimate  $-s_i/\sigma$ ,  $-s_j/\sigma$ ,

---

<sup>2</sup>Do not confuse  $\varepsilon$  with the one used in Section 4.2.1.

and  $\rho_{i,j}$ , we can estimate  $\sigma_P$  and its accuracy interval using the general method.

We denote model parameters by  $v$ ,  $w$ ,  $\theta$ , and  $z$ . Each notation means

$$\begin{aligned} v &= -s_i/\sigma, \\ w &= -s_j/\sigma, \\ \theta &= \rho_{i,j}, \\ z &= \sigma_P. \end{aligned}$$

We can directly estimate  $v, w$ , and  $\theta$  from experimental results  $y_i$ ,  $y_j$  and  $y_{i,j}$  as follows.

$$\begin{aligned} \hat{v} &= Q^{-1}(y_i), \\ \hat{w} &= Q^{-1}(y_j), \\ \hat{\theta} &= y_{i,j}. \end{aligned}$$

Using the estimates  $\hat{v}$ ,  $\hat{w}$ , and  $\hat{\theta}$ , we can calculate the estimate of  $z$  as

$$\hat{z} = P^\leftarrow(\hat{v}, \hat{w}, \hat{\theta}). \quad (4.11)$$

We denote estimation errors  $\hat{v} - v$ ,  $\hat{w} - w$ ,  $\hat{\theta} - \theta$ , and  $\hat{z} - z$  by  $\Delta v$ ,  $\Delta w$ ,  $\Delta \theta$ , and  $\Delta z$ , respectively.

We assume that each parameter has an accuracy interval with an upper-bounded error probability. If we denote the error probabilities by  $p_v$ ,  $p_w$ , and  $p_\theta$ , then

$$\begin{aligned} p_v &\geq Prob(|\Delta v| = |\hat{v} - v| \geq \varepsilon_v), \\ p_w &\geq Prob(|\Delta w| = |\hat{w} - w| \geq \varepsilon_w), \\ p_\theta &\geq Prob(|\Delta \theta| = |\hat{\theta} - \theta| \geq \varepsilon_\theta). \end{aligned} \quad (4.12)$$

We assume that  $\varepsilon_v, \varepsilon_w$ , and  $\varepsilon_\theta$  are sufficiently small.

Using partial derivatives,  $\hat{z}$  can be approximated to

$$\begin{aligned}\hat{z} &= P^\leftarrow(\hat{v}, \hat{w}, \hat{\theta}) \\ &= P^\leftarrow(v + \Delta v, w + \Delta w, \theta + \Delta \theta) \\ &\approx P^\leftarrow(v, w, \theta) + \Delta v \frac{\partial}{\partial v} P^\leftarrow(v, w, \theta) + \Delta w \frac{\partial}{\partial w} P^\leftarrow(v, w, \theta) + \Delta \theta \frac{\partial}{\partial \theta} P^\leftarrow(v, w, \theta).\end{aligned}$$

We derive the upper-bound of  $|\Delta z|$  as follows.

$$\begin{aligned}|\Delta z| &= |\hat{z} - z| = |\hat{z} - P^\leftarrow(v, w, \theta)| \\ &= \Delta v \frac{\partial}{\partial v} P^\leftarrow(v, w, \theta) + \Delta w \frac{\partial}{\partial w} P^\leftarrow(v, w, \theta) + \Delta \theta \frac{\partial}{\partial \theta} P^\leftarrow(v, w, \theta) \\ &\leq |\Delta v| \cdot \left| \frac{\partial}{\partial v} P^\leftarrow(v, w, \theta) \right| + |\Delta w| \cdot \left| \frac{\partial}{\partial w} P^\leftarrow(v, w, \theta) \right| + |\Delta \theta| \cdot \left| \frac{\partial}{\partial \theta} P^\leftarrow(v, w, \theta) \right| \\ &\leq \varepsilon_v \left| \frac{\partial}{\partial v} P^\leftarrow(v, w, \theta) \right| + \varepsilon_w \left| \frac{\partial}{\partial w} P^\leftarrow(v, w, \theta) \right| + \varepsilon_\theta \left| \frac{\partial}{\partial \theta} P^\leftarrow(v, w, \theta) \right|.\end{aligned}$$

The first inequality holds by the triangle inequality. The second inequality holds when estimation errors  $|\Delta v|$ ,  $|\Delta w|$ , and  $|\Delta \theta|$  are less than the width of accuracy intervals  $\varepsilon_v$ ,  $\varepsilon_w$ , and  $\varepsilon_\theta$ , respectively. From Eqn. (4.12), these inequalities hold with at least  $(1 - p_v)(1 - p_w)(1 - p_\theta)$  probability.

If we define  $\varepsilon_z$  as

$$\varepsilon_z = \varepsilon_v \left| \frac{\partial}{\partial v} P^\leftarrow(v, w, \theta) \right| + \varepsilon_w \left| \frac{\partial}{\partial w} P^\leftarrow(v, w, \theta) \right| + \varepsilon_\theta \left| \frac{\partial}{\partial \theta} P^\leftarrow(v, w, \theta) \right|,$$

then we can formulate the accuracy interval and its probability of the model parameter  $z$  by

$$Prob(|z - \hat{z}| \leq \varepsilon_z) \geq (1 - p_v)(1 - p_w)(1 - p_\theta) = 1 - p_z, \quad (4.13)$$

where  $p_z$  is defined as the upper-bound of the error probability of the accuracy interval.

Assuming that  $\varepsilon_v, \varepsilon_w, \varepsilon_\theta$  are sufficiently small, we approximate  $\varepsilon_z$  to

$$\varepsilon_z \approx \varepsilon_v \left| \frac{\partial}{\partial v} P^\leftarrow(\hat{v}, \hat{w}, \hat{\theta}) \right| + \varepsilon_w \left| \frac{\partial}{\partial w} P^\leftarrow(\hat{v}, \hat{w}, \hat{\theta}) \right| + \varepsilon_\theta \left| \frac{\partial}{\partial \theta} P^\leftarrow(\hat{v}, \hat{w}, \hat{\theta}) \right|. \quad (4.14)$$

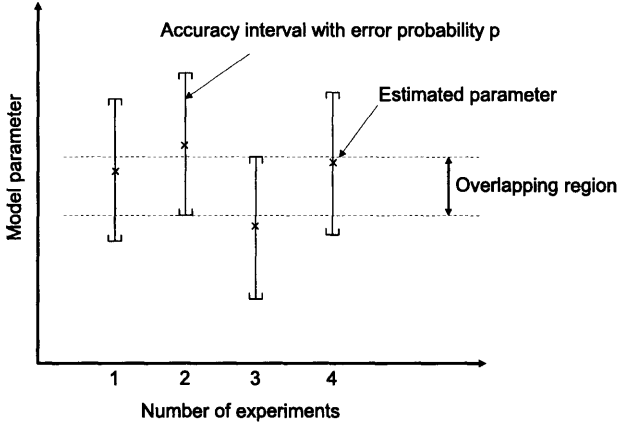


Figure 4-1: Accuracy intervals and their overlapping region.

Thus, we can calculate  $\varepsilon_z$  of the parameter  $z$  from  $\varepsilon_v$ ,  $\varepsilon_w$ ,  $\varepsilon_\theta$ , and partial derivatives. The error probability of the accuracy interval can be evaluated from  $p_v$ ,  $p_w$ , and  $p_\theta$  using Eqn. (4.13).

### The existence of an overlap region in repeated independent experiments

From  $n$  repeated independent experiments, we can plot the estimates of a model parameter and their accuracy intervals. Figure 4-1 shows the figure of accuracy intervals. In this figure, the x-axis denotes an experiment number and the y-axis means the value of the model parameter. For each experiment, we draw an accuracy interval parallel to y-axis.

From the figure, we can check the existence of an overlapping region of all  $n$  accuracy intervals. Let  $p_i$  be the upper-bound of an error probability of an accuracy interval  $i$ . If the model is correct, then the probability of existence of the overlap region among  $n$  accuracy intervals is  $\prod_{i=1}^n (1-p_i)$  since all experiments are independent of each other.

The correctness of model assumptions can be verified from existence of this overlapping region. In our model, we assumed that delays are additive. The distributions

of  $\Delta_i(c)$  and  $p_i(c)$  are independent of each other as well as Gaussian. Let  $p_o$  be the probability of existence of an overlap region. If an overlap does not exist when  $p_o$  is close to 1, we conclude that the experimental results do not follow the model assumptions. Thus, we must extend the model to consider unknown non-linearity. We measure an amount of non-linearity using the suggested model in Section 4.1.2.

### 4.2.3 Estimation of $\sigma_\Delta/\sigma_p$ using a Non-linear Delay Model

In this section, we re-calculate the accuracy intervals of  $\sigma_P$  estimates using the non-linear delay model. Intuitively, adding a non-linearity factor to a linear delay model will give an extra margin to the accuracy interval.

Similar to Section 4.2.2, we formulate the probability  $Prob(R_j(c) = 1, R_i(c) = 1)$  considering the non-linearity factor  $\gamma$ .

$$\begin{aligned} \rho_{i,j} &= Prob(R_j(c) = 1, R_i(c) = 1) \\ &= Prob(s_j + \Delta(c) + p_j(c) + \gamma \leq 0, s_i + \Delta(c) + p_i(c) + \gamma \leq 0) \\ &= Prob\left(\frac{p_j(c)}{\sigma_p} \leq A_j, \frac{p_i(c)}{\sigma_p} \leq A_i\right). \end{aligned} \quad (4.15)$$

where

$$A_i = -\frac{s_i}{\sigma} \sqrt{1 + \sigma_P^2} - \frac{\Delta(c)}{\sigma_\Delta} \sigma_P - \gamma/\sigma_p.$$

We define a normalized non-linearity factor as

$$\gamma' = \gamma/\sigma_p.$$

Then, from Eqn. (4.3),

$$-R' \leq \gamma' \leq R',$$

where  $R' = R/\sigma_p$ . Using  $-\sigma_i/\sigma$ ,  $-\sigma_j/\sigma$ ,  $\sigma_P$ , and  $\gamma'$ , we derive  $\rho_{i,j}$  as follows.

$$\begin{aligned}\rho_{i,j} &= \int_{t=-\infty}^{\infty} \frac{e^{-t^2/2}}{\sqrt{2\pi}} Q(-(s_j/\sigma)\sqrt{1+\sigma_P^2} - t\sigma_P - \gamma') Q(-(s_i/\sigma)\sqrt{1+\sigma_P^2} - t\sigma_P - \gamma') dt \\ &= P_2(-s_i/\sigma, -s_j/\sigma, \sigma_P, \gamma'),\end{aligned}$$

where

$$P_2(v, w, z, r) = \int_{t=-\infty}^{\infty} \frac{e^{-t^2/2}}{\sqrt{2\pi}} Q(v\sqrt{1+z^2} - tz - r) Q(w\sqrt{1+z^2} - tz - r) dt$$

As solutions of  $\theta = P_2(v, w, z, r)$ ,

$$z = P_2^\leftarrow(v, w, \theta, r).$$

Similar to Section 4.2.2, we can use a simple binary search to evaluate  $P_2^\leftarrow(v, w, \theta, r)$  when  $v, w, \theta$ , and  $r$  are given.

We use the same notations  $v$ ,  $w$ ,  $\theta$ , and  $z$  for the model parameters  $-s_i/\sigma$ ,  $-s_j/\sigma$ ,  $\rho_{i,j}$ , and  $\sigma_P$ . We add  $r$ , which means the normalized non-linearity  $\gamma'$ , to the model. From the definition of  $\gamma$ ,

$$p_r = Prob(|r| \geq R') = 0.$$

Assuming that  $R'$  is sufficiently small, we derive the accuracy interval width  $\varepsilon_z$  similar to Section 4.2.2 as follows.

$$\begin{aligned}\varepsilon_z &\approx \varepsilon_v \left| \frac{\partial}{\partial v} P_2^\leftarrow(\hat{v}, \hat{w}, \hat{\theta}, 0) \right| + \varepsilon_w \left| \frac{\partial}{\partial w} P_2^\leftarrow(\hat{v}, \hat{w}, \hat{\theta}, 0) \right| \\ &\quad + \varepsilon_\theta \left| \frac{\partial}{\partial \theta} P_2^\leftarrow(\hat{v}, \hat{w}, \hat{\theta}, 0) \right| + R' \left| \frac{\partial}{\partial r} P_2^\leftarrow(\hat{v}, \hat{w}, \hat{\theta}, 0) \right|.\end{aligned}\tag{4.16}$$

Compared to Eqn. (4.14), the non-linearity term  $R' \left| \frac{\partial}{\partial r} P_2^\leftarrow(\hat{v}, \hat{w}, \hat{\theta}, 0) \right|$  has been added to give an extra margin to the accuracy interval. Since  $p_r = 0$ , the error probability of the accuracy interval does not change.

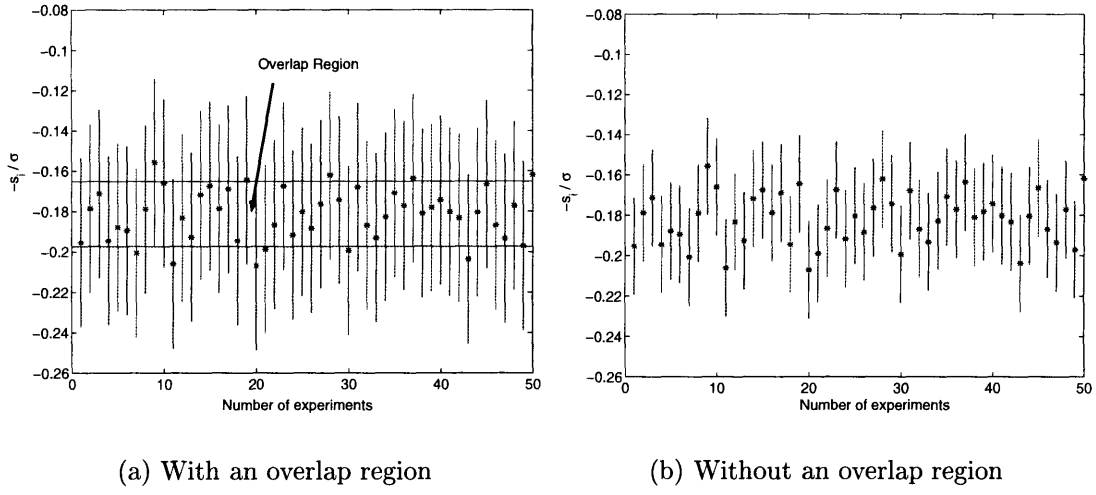


Figure 4-2: Estimated skew parameters and their accuracy intervals from independent experiments.

## 4.3 Experiments

### 4.3.1 Estimation of $s_i$

Before generating CRPs of a PUF, we compensate for the skew in each PUF by fixing 12 of the most significant bits of a challenge vector (cf. Section 3.2.3). Using the compensated PUFs we generate 10,000 CRPs by using random challenges. From Eqn. (4.4), we calculate  $y_i$ , the estimate of  $\rho_i$ . We repeat this experiment 50 times to obtain 50  $y_i$ 's and estimate  $-s_i/\sigma$  by evaluating  $Q^{-1}(y_i)$ .

Figure 4-2(a) shows 50 estimates of  $-s_i/\sigma$  for a compensated PUF  $i$  and their accuracy intervals. For each accuracy interval, the error probability  $Prob(|-s_i/\sigma - Q^{-1}(y_i)| > \delta)$  is less than 0.001. Each accuracy interval width  $\delta$  has been evaluated by Eqn. (4.7). From the figure, the estimated  $-s_i/\sigma$  is  $-0.18$ .

To verify the correctness of the skew model, we observe the existence of an overlapping region between accuracy intervals. The probability of existence of an overlap region between 50 accuracy intervals is greater than or equal to  $0.999^{50} \approx 0.95$ . Since the overlap exists in Figure 4-2(a), this result is well-suited to our model.

Figure 4-2(b) shows non-existence of an overlap region when we decrease the accuracy interval width until the overlap disappears. The error probability of each

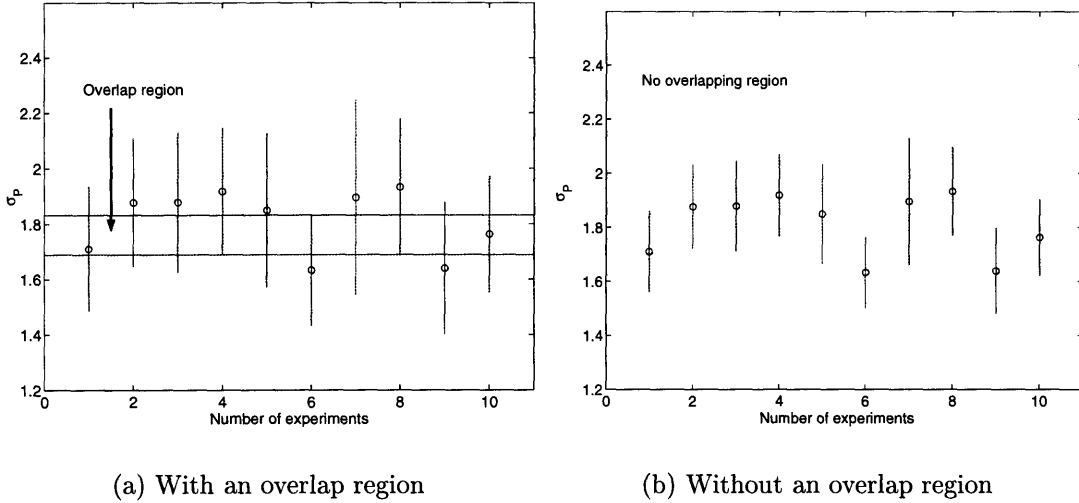


Figure 4-3: Estimated  $\sigma_P$  and their accuracy intervals from independent experiments.

accuracy interval is 5.74%. Since the probability of existence of an overlap  $p_o$  is only  $0.9426^{50} = 0.052$ , This result does not contradict our model. Thus, we conclude that a skew in each PUF can be estimated consistently using the linear delay model. The estimate and accuracy interval of a skew can be used in estimating other model parameters.

### 4.3.2 Estimation of $\sigma_\Delta/\sigma_p$

To estimate  $\sigma_P$ , we use 10 independent pairs of two different PUFs. For each pair, we generate 20,000 CRPs and calculate  $y_i$  and  $y_j$  to estimate the skews of two PUFs. Using Eqn. (4.9), we estimate  $\rho_{i,j}$  by evaluating  $y_{i,j}$ . These three estimates  $y_i$ ,  $y_j$ , and  $y_{i,j}$  are used to estimate  $\sigma_P$ .

Figure 4-3(a) shows the estimates of  $\sigma_P$  and their accuracy intervals in 10 repeated experiments. These experiments are independent of each other. The estimates of  $\sigma_P$  have been calculated by Eqn. (4.11) and their accuracy intervals have been evaluated by Eqn. (4.14). In this figure, the error probability of each accuracy interval is 0.3497. The estimated  $\sigma_P$  is around 1.75, which means that  $\sigma_\Delta$  is only 1.75 times larger than the process variation  $\sigma_p$ .

We can verify the existence of overlap region  $L = [1.68, 1.83]$  from the figure. Since 10 independent experiments were performed, the probability of the existence of an overlap region is 1.35%. The existence of this overlap means that experimental results are well-suited to our model. In other words, the estimates of repeated experiments are sufficiently consistent, and therefore, we can obtain the accurate estimate of  $\sigma_P$ . We do not need to introduce non-linearity to give an extra margin to accuracy intervals.

To verify our model, we decrease the accuracy interval widths until the overlap does not exist. Figure 4-3(b) shows the non-existence of the overlap when the error probability of each accuracy interval is 68.65%. In this case,  $p_o$  is only  $7.5 \cdot 10^{-6}$ . Since  $p_o$  is extremely small, the experimental results do not contradict our model.

### 4.3.3 Estimation of Non-linearity

We estimate non-linearity in experimental results using the non-linear delay model in Section 4.1.2. Assuming that  $\gamma = 0$ , we estimate a model parameter based on the original linear delay model. We denote  $p_t$  as the error probability of an accuracy interval when there is no overlap between accuracy intervals of estimates. Then, we introduce the non-linearity  $\gamma > 0$  to the model and increase the maximum value of normalized non-linearity  $R'$  until we gain the overlap. The increase of  $R'$  enlarge the width of accuracy interval following the definition of Eqn. (4.16). We denote  $R'_t$  as the minimum required non-linearity to gain the overlap region.

To prove our non-linear delay model, we have tested the non-linearity of PUF responses from the simulation of two different arbiter-based PUF models. The first model is an additive delay model without non-linear noise. We assume that every delay segment in an arbiter circuit is a constant and the process variation in each delay component is Gaussian. From the additive delay model in Section 5.2.1, we model the delay difference between top and bottom paths as the inner product of the random challenge vector  $\mathbf{c}$  and the constant delay vector  $\mathbf{d}_i$ . The delay vector  $\mathbf{d}_i$  is composed of a common delay vector  $\mathbf{d}$  and process variation vector  $\mathbf{p}_i$ . The common delay vector  $\mathbf{d}$  consists of the delay values of circuit components without considering

process variation. Each component of a process variation vector  $\mathbf{p}_i$  is a zero-mean Gaussian. We set  $\sigma_P$ , which can be represented as  $\frac{\|\mathbf{d}\|}{\|\mathbf{p}_i\|}$  (cf. Section 4.4), to two. There is no arbiter skew and measurement noise in this model.

The second model is an additive delay model with non-linear noise. The noise source  $N$  is added at the end of delay paths to introduce non-linear random noise to the model. As an example of non-linear random noise, we use random numbers from  $\chi^2$ -distribution. For  $X \sim \chi^2(v, 1)$ , where  $v = 20$ , we define  $N$  as

$$N = \frac{X - v}{3v}, \text{ where } v = 20.$$

The mean and standard deviation of  $N$  are a zero and  $\sigma_\Delta/10$ , respectively. This model does not have an arbiter skew and  $\sigma_P = 2$ .

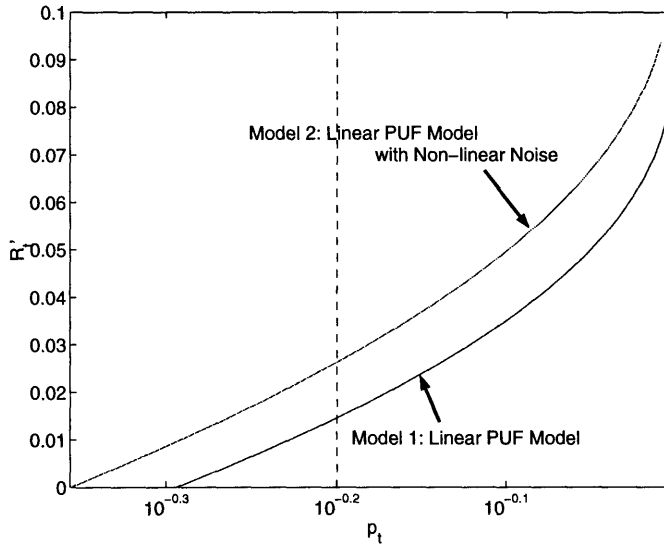


Figure 4-4: Comparison of  $p_t - R'_t$  curves depending on the existence of non-linear noise.

Figure 4-4 shows the  $p_t - R'_t$  curves from simulated responses of the first and second models. Since the two models have the same amount of process variation  $\sigma_p$ , we can directly compare the non-linearity  $R'_t$ , which is normalized with  $\sigma_p$ . From the figure, the first model requires more non-linearity than the second model to fit the experimental results to the linear delay model. This result follows the fact that the second model has more non-linear random noise that cannot be predicted by

a linear algorithm than the first model. When an adversary is willing to build a software model to predict responses, the second model is more difficult to break than the first model since the random noise causes prediction errors. Thus, the measured non-linearity from this method is related to the modeling complexity of arbiter-based PUFs. We exploit this method to analyze the security of alternative types of PUFs in Chapter 6.

## 4.4 Identification/Authentication Capability

We study the identification/authentication capability of arbiter-based PUFs based on inter-chip variation  $\tau$  and noise probability  $\mu$ . Since environmental variation is the primary factor of noise, we consider only environmental variation for noise in this section. We represent the identification/authentication capability by the probability of errors that can occur in identifying/authenticating billions of PUFs. In the calculation of the error probability, we assume that CRP measurements are independent of each other. Since  $\tau$  and  $\mu$  are related to the number of PUF delay stages  $m$ , we calculate appropriate  $m$  to gain the desired  $\tau$  and  $\mu$  using our delay model.

### 4.4.1 Inter-chip Variation and Environmental Variation

We study how inter-chip variation and environmental variation are related to the number of delay stages. Based on the delay model in this Chapter, we represent  $\tau$  and  $\mu$  as the function of  $m$ . When  $m$  is sufficiently large, the skew of an arbiter does not affect PUF responses. Using the model, we evaluate the inter-chip variation and environmental variation without the arbiter skew.

#### Information-bearing challenges

We can estimate the number of information-bearing challenges in the complete set of challenges using a linear model of an arbiter-based PUF. Let  $k$  be the number of arbiter-based PUFs. We denote the probability of a random challenge  $c$  being an information-bearing challenge by  $\eta$ . We do not consider skew in the arbiter. Using

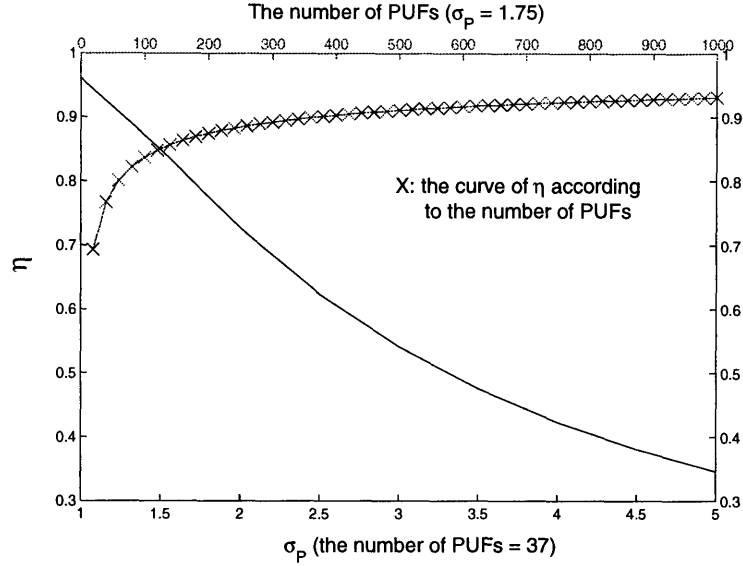


Figure 4-5: The change of  $\eta$  according to the number of PUFs and  $\sigma_P$ .

$\sigma_P$ , we can derive  $\eta$  as follows.

$$\begin{aligned}\eta &= 1 - \text{Prob}(R_i(c) = 1 \text{ for all } 1 \leq i \leq k) - \text{Prob}(R_i(c) = 0 \text{ for all } 1 \leq i \leq k) \\ &= 1 - \int_{-\infty}^{\infty} \frac{e^{-t^2/2}}{\sqrt{2\pi}} \left( \int_{-\infty}^{t\sigma_P} \frac{e^{-v^2/2}}{\sqrt{2\pi}} dv \right)^k dt - \int_{-\infty}^{\infty} \frac{e^{-t^2/2}}{\sqrt{2\pi}} \left( \int_{t\sigma_P}^{\infty} \frac{e^{-v^2/2}}{\sqrt{2\pi}} dv \right)^k dt. \quad (4.17)\end{aligned}$$

Using the estimate of  $\sigma_P$  ( $\approx 1.75$ ) in Section 4.3.2, we can calculate the number of information-bearing challenges. From Eqn. (4.17), when  $k = 37$ ,  $\eta = 0.8204$ . This means that 82.04% of total challenges are information-bearing challenges. In Section 3.3.1, we verified that around 80% of total challenges are information-bearing challenges in our 37 test-chips, which is similar to the computed  $\eta$ . We conclude that the number of information-bearing challenges can be calculated from Eqn. (4.17).

Figure 4-5 shows the change of  $\eta$  according to the number of PUFs and  $\sigma_P$ . When there are more than 1,000 of PUFs, the portion of information-bearing challenges converges to 93%. To obtain more information-bearing challenges, we must place and route delay components symmetrically to reduce  $\sigma_P$ .

## Inter-chip variation

The inter-chip variation  $\tau$  between two different PUFs is defined as

$$\tau = \text{Prob}(R_i(c) \neq R_j(c)),$$

where  $i \neq j$  and  $c$  is a random challenge. We can evaluate  $\tau$  using given model parameters  $-s_i/\sigma$ ,  $-s_j/\sigma$ , and  $\sigma_P$  as follows.

$$\tau = T(-s_i/\sigma, -s_j/\sigma, \sigma_P), \quad (4.18)$$

where

$$\begin{aligned} T(v, w, z) &= \int_{t=-\infty}^{\infty} \frac{e^{-t^2/2}}{\sqrt{2\pi}} ((1 - Q(v\sqrt{1+z^2} - tz))Q(w\sqrt{1+z^2} - tz) \\ &\quad + Q(v\sqrt{1+z^2} - tz)(1 - Q(w\sqrt{1+z^2} - tz))) dt. \end{aligned}$$

We represent  $\tau$  as the function of  $m$ , which is the number of delay stages. Let  $p_{ij}(c)$  be the process variation in the  $j$ th stage of PUF  $i$ . By the Gaussian assumption of process variation,

$$p_{ij}(c) \sim N(0, \sigma_{p'}).$$

We assume that  $\sigma_{p'}$  is constant for every stage. Since delays are additive, we model

$$p_i(c) = \sum_{j=1}^m p_{ij}(c).$$

Since  $p_{ij}(c)$ 's are independent of each other,

$$\sigma_p = \sqrt{m}\sigma_{p'}.$$

We represented  $\Delta(c)$ , which is the delay difference between top and bottom paths without process variation, as  $\langle \mathbf{d}, \mathbf{c} \rangle$ , where  $\mathbf{d} = (d_1, d_2, \dots, d_m)$  is a constant vector and  $\mathbf{c} = (c_1, c_2, \dots, c_m)$  is a random challenge vector for  $c_i \in \{-1, 1\}$ . Assuming that

$m$  is sufficiently large, we can model

$$\Delta(c) \sim N(0, \sigma_\Delta),$$

by the Central Limit Theorem. We denote  $\sigma_{c_i}$  as the standard deviation of  $c_i$ . Since  $c_i \in \{-1, 1\}$  and a uniform random variable,  $\sigma_{c_i} = 1$ . We represent  $\sigma_\Delta$  using  $\mathbf{d}$  as follows.

$$\sigma_\Delta = \sqrt{\sum_{i=1}^m d_i^2 \sigma_{c_i}^2} = \sqrt{\sum_{i=1}^m d_i^2} = \|\mathbf{d}\|.$$

Assuming that every delay stage is identical, we can approximate

$$\sigma_\Delta \propto \sqrt{m}.$$

Since both  $\sigma_p$  and  $\sigma_\Delta$  are proportional to  $\sqrt{m}$ ,  $\sigma = \sqrt{\sigma_\Delta^2 + \sigma_p^2}$ , which is the delay difference between top and bottom paths with process variation, is also proportional to  $\sqrt{m}$ .

From Eqn. (4.18),  $\tau$  can be represented as the function of  $-s_i/\sigma$ ,  $-s_j/\sigma$ , and  $\sigma_P$ . Let  $S_i$  be the skew  $-s_i/\sigma$  when  $m = 64$  for PUF  $i$ . We can estimate  $S_i$  from experiments (cf. Section 4.3.1). Since  $\sigma$  is proportional to  $\sqrt{m}$ , we represent the skew  $-s_i/\sigma$  as a function of  $m$  as follow:

$$-s_i/\sigma = \frac{8S_i}{\sqrt{m}}.$$

Since both  $\sigma_\Delta$  and  $\sigma_p$  are proportional to  $\sqrt{m}$ ,  $\sigma_P = \sigma_\Delta/\sigma_p$  is a constant to  $m$ . We conclude that

$$\tau(m) = T\left(\frac{8S_i}{\sqrt{m}}, \frac{8S_j}{\sqrt{m}}, \sigma_P\right),$$

where  $S_i$  and  $S_j$  are estimated skews from PUF  $i$  and  $j$ , respectively.

Figure 4-6 shows the curve of inter-chip variation  $\tau$  as a function of  $m$ . For two different PUFs, we estimate the skews  $S_i$  and  $S_j$  and  $\sigma_P$  (cf. Section 4.3). Based

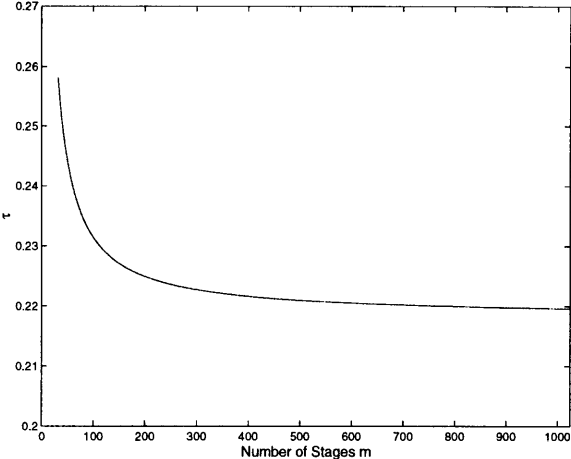


Figure 4-6: The change of  $\tau$  according to the number of the stages in delay paths.

on these parameters, we calculate  $\tau$  when  $m$  varies from 32 to 1024. Intuitively, the inter-chip variation  $\tau$  decreases according to the increase of  $m$  because the influence of the skews decreases while  $\sigma_P$  remains constant. From the curve,  $\tau$  converges to 0.22, which is the inter-chip variation of arbiter-based PUFs that have no arbiter skew.

### Environmental variation

While we cannot find any appropriate model to represent the noise of PUF responses as a function of  $m$ , we can roughly examine the relationship between the noise and the number of stages  $m$ . At first, we consider measurement noise of arbiter-based PUFs. Section 3.3 shows that the setup time ( $t_{su}$ ) of an arbiter causes measurement noise. When  $\Delta_i(c)$  is less than  $t_{su}$ , the arbiter is in a meta-stable state and the response of the arbiter is unreliable. Thus, measurement noise  $\mu_m$  is proportional to  $Prob(|\Delta_i(c)| \leq t_{su})$ .

In our model,  $\Delta_i(c) \sim N(s_i, \sigma)$ . When  $m$  is sufficiently large, we can approximate  $s_i \approx 0$ .

$$\mu_m \propto Prob(|x| \leq t_{su}), \text{ where } x \sim N(0, \sigma).$$

We already verified that  $\sigma$  is proportional to  $\sqrt{m}$ . When we increase  $m$ ,  $\mu_m$  decreases

because the increase of  $\sigma$  reduces  $Prob(|x| \leq t_{su})$ . Table 4.1 shows experimental results. We used FPGAs to change  $m$  in the PUF circuit. From the table, we can verify that the measurement noise decreases according to the increase of  $m$ .

The number of stages ( $m$ )	Measurement noise(%)
32	0.106
64	0.086
96	0.078
128	0.074

Table 4.1: Measurement noises in the different number of stages.

Similarly, we can expect that environmental variation decreases according to the increase of  $m$ . Let's assume that environmental variation on PUF circuits increases or decreases  $\Delta_i(c)$  by  $\delta(c)$ . If we denote  $t_{en}$  as the maximum value of  $|\delta(c)|$ , environmental variation  $\mu$  is proportional to  $Prob(|\Delta_i(c)| \leq t_{en})$ . Therefore, using the same arguments in the measurement noise analysis, we can conclude that the increase of  $m$  decreases  $\mu$ . The maximum environmental variation 4.84% from experimental results (cf. Section 3.3) can be decreased by increasing the number of stages. We use  $\mu = 0.0484$  as the worst case environmental variation in the calculation of identification/authentication capability in the next section.

#### 4.4.2 Identification/Authentication Capability

Given the inter-chip variation  $\tau$  and environmental variation  $\mu$ , we can evaluate the identification/authentication capability of arbiter-based PUFs. We represent this capability as the probability of errors that can occur in identifying/authenticating billions of PUFs. Since the error probability can be reduced by using a larger number of CRPs, we calculate the number of CRPs to make the error probability sufficiently small ( $< 10^{-9}$ ).

For convenience, we define two probabilities,  $p_d(t, k)$  and  $p_n(t, k)$ . When inter-chip variation is  $\tau$ , the probability that at least  $t$  out of  $k$  reference responses differ

between two different chips is equal to

$$p_d(t, k) = 1 - \sum_{i=0}^{t-1} \binom{k}{i} \tau^i (1-\tau)^{k-i}. \quad (4.19)$$

For a single chip, when environmental variation is  $\mu$ , the probability that at most  $t$  out of  $k$  responses differ from the corresponding reference responses is

$$p_n(t, k) = 1 - \sum_{j=t+1}^k \binom{k}{j} \mu^j (1-\mu)^{k-j}. \quad (4.20)$$

## Identification

When we use PUFs for the identification of registered users, there exists the server that stores CRP profiles of  $N$  registered PUFs in its database. Each CRP profile has  $k$  CRPs. When a user presents a PUF to the server, the server generates CRPs using the presented PUF and compares it with all CRP profiles of the registered users in the database. The server identifies the user by finding the minimum distance CRP profile from the generated CRPs of the presented PUF.

In this scheme, the probability of error is equal to

$$p_e = 1 - \sum_{i=0}^{k-1} \binom{k}{i} \mu^i (1-\mu)^{k-i} (p_d(i+1, k))^{N+1}, \quad (4.21)$$

where  $p_d(i, k)$  is the probability defined in Eqn. (4.19). We use  $\tau = 0.22$  and  $\mu = 0.048$  from experimental results (cf. Section 3.3). When  $N = 10^9$ , we need  $k > 450$  to achieve  $p_e \leq 10^{-9}$ .

This result shows that we can identify  $10^9$  PUFs with only 450 CRPs. The error probability in this identification is less than  $10^{-9}$ . However, this scheme is not practical because the comparison with all CRPs in database imposes a significant performance overhead. Furthermore, we cannot distinguish a non-registered PUF since we always choose the minimum distance profile in the database.

## Authentication

To avoid the comparison with all CRP profiles in database, the server first asks the user-name of the presented key-card and authenticates the PUF in the key-card by profile matching. This scheme is significantly faster than simple identification because the server needs to perform profile matching only once.

In the authentication of a PUF, the server compares the CRPs of a presented PUF with the CRP profile of a presented user-name in database. If the distance between two CRP profiles is less than or equal to the threshold  $t$ , the server authenticate the PUF. Otherwise, this access is rejected by the server.

In this scheme, two kinds of errors are possible.

**Robustness:** A user presents a valid PUF, but a server recognizes it as a wrong PUF. The probability of this error  $p'_e$  is equal to

$$p'_e = \sum_{i=t+1}^k \binom{k}{i} \mu^i (1-\mu)^{k-i} = 1 - b(t).$$

We can see that  $p'_e$  decreases monotonically when  $t$  increases.

**Security:** When an adversary issues a wrong PUF to a server, the server authenticates it by mistake. The probability of this error is

$$p''_e = \sum_{i=0}^t \binom{k}{i} \tau^i (1-\tau)^{k-i}.$$

Clearly,  $p''_e$  increases monotonically when  $t$  increases.

In  $n$  uses of authentication, we assume that an adversary tries to deceive a key-card server by issuing a wrong PUF  $d$  times. We denote  $\alpha = d/n$  as the frequency of the deceiving trials. The system error probability  $p_e$  can be represented using  $\alpha$  as follows.

$$p_e = (1-\alpha)p'_e + \alpha p''_e. \quad (4.22)$$

Assuming  $\alpha = 0.5$ , our goal is to achieve  $p_e \leq 10^{-9}$  using a minimum  $k$  and an appropriate  $t$ . Similar to identification, we use  $\tau = 0.22$  and  $\mu = 0.048$ . From calculation,  $p_e = 9.3 \cdot 10^{-10} < 10^{-9}$  when  $k = 443$  and  $t = 48$ . We conclude that using less than 450 CRPs we can authenticate the PUF with negligible error probability.



# Chapter 5

## Breaking an Arbiter-Based PUF

Since an arbiter-based PUF exploits inevitable process variation in the manufacturing of ICs, the PUF cannot be duplicated by an adversary even with the detailed knowledge of a circuit. However, attacks to break arbiter-based PUFs are still possible. For example, an adversary can build a timing accurate model to simulate the PUF circuit. Moreover, if there exists notable correlation between challenges and responses, then an adversary can build a software model of the PUF and use it as a “virtual counterfeit”. The security of physical random functions is based on the difficulty of response prediction (cf. Chapter 2). Therefore, these types of modeling attacks can be critical threats to the security of arbiter-based PUFs.

In Section 5.1, we provide possible invasive and non-invasive attack models on arbiter-based PUFs. Among the possible attack models, we provide the software model building attack based on a machine learning algorithm called *Support Vector Machine* in Section 5.2. We show how to train the algorithm using a polynomial number of CRPs and verify the prediction accuracy of the trained algorithm using FPGAs and custom silicon in Section 5.3.

### 5.1 Attack Models

In this section, we introduce possible attack models on arbiter-based PUFs. Most of the attacks were already introduced in [2] based on the PUF that uses a *MAX*

circuit instead of an arbiter. Though we use a different type of a PUF, an adversary can use the same attacks since both arbiter-based PUFs and *MAX*-based PUFs use the same delay path structure.

### 5.1.1 Duplication

If an adversary can fabricate a “counterfeit” PUF, which is logically identical with the original PUF, he can break the authentication methodology. The term “logically identical” means that a counterfeit PUF produces almost the same responses as the original PUF for most of random challenges. A special case of this attack occurs when an IC manufacturer attempts to produce two identical ICs from scratch.

Given the statistical variation inherent in manufacturing process we used, we argue that it is impossible to produce an IC precisely enough to control the PUF that the IC embodies. When producing two ICs in identical conditions (same production line, same position on wafer, etc.), the manufacturing variations are still sufficient to yield two significantly different PUFs. We have tested the PUFs from the same wafer and verified that inter-chip variation is sufficient to identify each PUF in Section 3.3.

Following the identification capability discussion in Section 4.4, the probability that two different PUFs are indistinguishable from each other is extremely low. Thus, an adversary must fabricate a huge number of ICs and make comprehensive measurements on each one in order to discover a match. This is a very expensive proposition, both from economical and computational standpoint.

### 5.1.2 Timing-Accurate Model Building

Today, the accuracy of measurement devices is getting more precise. Though process variation in the manufacturing of ICs is beyond the control of a manufacturer, by measuring delays of all circuit components, an adversary can create a time-accurate model of an original PUF and simulate the model to predict the responses of randomly given challenges. The success of this timing-accurate model depends on the accuracy of the measurement devices.

## **Direct Measurement**

The development of reverse engineering techniques has made it possible to extract the important circuit information such as circuit topology and a physical dimension of each component (cf. Chapter 1). It is also possible to directly measure the delays of circuit components by micro-probing. These measured delays can be used to construct a sophisticated timing model.

In order for this delay measurement to be at the level of the accuracy required to break authentication, an adversary must remove the package of an IC and insert probes. Alternatively, he can use non-invasive attacks such as differential power analysis [12] and electromagnetic analysis [17] to extract information about collections of devices. However, probing with sufficient precision is significantly difficult because the delay of the probing device will change the measured delays. Interactions between the probe and the circuit can introduce noise in the measurement. Moreover, in order to insert his probes, the adversary may damage overlaid wires. Because of the high capacitive coupling between neighboring wires (cf. [6] for the importance of capacitive coupling between wires), damage to these overlaid wires could change the delays that are being measured. To make the direct measurement more difficult, the circuit can be protected by a tamper-sensing environment. How best to layout the PUF circuit to make it highly sensitive to invasive attacks is a direction for future research.

## **Exhaustive Model**

Clearly, a model can be built by exhaustively enumerating all possible challenges. However, exhaustive modeling is intractable since there are an exponential number of possible challenges. In our test-chip, a challenge is 64 bits and it takes 50 ns for one measurement. By simple calculation, it takes more than 30,000 years to generate all CRPs.

### 5.1.3 Software Model Building Attacks

Non-invasive model building attacks are also possible. First, an adversary can use a publicly available mask description of IC/PUF to build a timing-accurate model with a polynomial number of parameters. In other words, an adversary can formulate the responses of a PUF as a function of challenges and circuit parameters. If the challenge-response model of the PUF circuit is linear, then an adversary can apply a polynomial number of random challenges and monitor the responses to estimate circuit parameters in the linear model. If the model can predict the response of the circuit with the error probability lower than the maximum environmental variation, the adversary can impersonate the original PUF with the model. We note that if the PUF has been calibrated in different environments (e.g., different temperatures), the adversary's job can be made harder.

In Section 3.3, we provided data on environmental variation and inter-chip variation of arbiter-based PUFs. When considering the model building attacks, we must calculate the probability of being deceived by possible software models from the prediction error probabilities of the models.

## 5.2 Software Modeling Building Attack: Support Vector Machines

We model a PUF circuit using an additive delay model. In this model, we assume that the delay of a path through the circuit is the sum of the delays of elementary components. Knowing all the elementary component delays, an adversary can predict responses for any challenge by calculating the circuit delay. The adversary's task is to estimate the elementary delay parameters. Assuming that direct measurement of the delays is impractical, the adversary can infer those delays from a polynomial number of CRPs using the machine learning algorithm named *Support Vector Machine*.

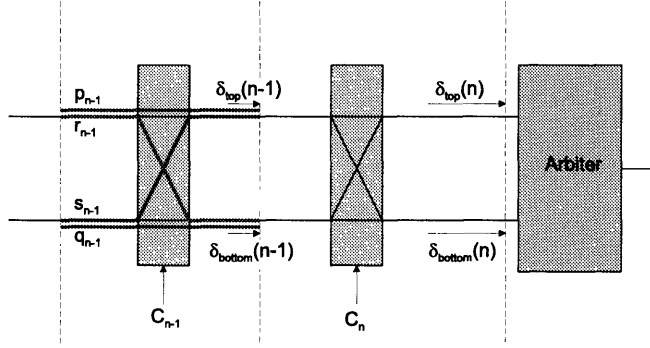


Figure 5-1: The notations of delay segments in each stage.

### 5.2.1 Additive Delay Model of a PUF Circuit

We denote  $\delta_{top}(n)$  as a signal delay from the starting point to the top path at the end of the  $n^{\text{th}}$  stage. Similarly,  $\delta_{bottom}(n)$  denotes the delay of the bottom path.

Figure 5-1 shows the notations of the delay segments  $p_n$ ,  $q_n$ ,  $r_n$ , and  $s_n$  in each stage. We can derive  $\delta_{top}(i+1)$  as a function of  $\delta_{top}(i-1)$ ,  $\delta_{bottom}(i-1)$ , and the delay segments of the  $i^{\text{th}}$  stage as follows.

$$\begin{aligned}\delta_{top}(i+1) = & \frac{1+C_{i+1}}{2}(p_{i+1} + \delta_{top}(i)) + \\ & + \frac{1-C_{i+1}}{2}(s_{i+1} + \delta_{bottom}(i))\end{aligned}\quad (5.1)$$

$$\begin{aligned}\delta_{bottom}(i+1) = & \frac{1+C_{i+1}}{2}(q_{i+1} + \delta_{bottom}(i)) + \\ & + \frac{1-C_{i+1}}{2}(r_{i+1} + \delta_{top}(i)),\end{aligned}\quad (5.2)$$

where  $C_i \in \{-1, 1\}$  is a challenge bit of the  $i^{\text{th}}$  stage.

Then, we denote  $\Delta(n)$  as the difference between  $\delta_{top}(n)$  and  $\delta_{bottom}(n)$ . By sub-

tracting Eqn. (5.2) from Eqn. (5.1), we can derive

$$\Delta(i+1) = C_{i+1} \cdot \Delta(i) + \alpha_{i+1}C_{i+1} + \beta_{i+1}, \quad (5.3)$$

where

$$\alpha_n = \frac{p_n - q_n + r_n - s_n}{2} \quad (5.4)$$

$$\beta_n = \frac{p_n - q_n - r_n + s_n}{2}. \quad (5.5)$$

We define the parity of challenge bits  $p_k$  as

$$p_k = \prod_{i=k+1}^n C_i,$$

where  $p_n = 1$ .

From Eqn. (5.3), we can represent  $\Delta(n)$  as a function of  $\alpha_i$ ,  $\beta_i$ , and  $C_i$  for  $1 \leq i \leq n$ , and simplify it using the parity  $p_i$  such that,

$$\begin{aligned} \Delta(0) &= 0 \\ \Delta(1) &= C_1 \cdot \Delta(0) + \alpha_1 C_1 + \beta_1 = \alpha_1 C_1 + \beta_1 \\ \Delta(2) &= C_2(\alpha_1 C_1 + \beta_1) + \alpha_2 C_2 + \beta_2 = \alpha_1 C_1 C_2 + \alpha_2 C_2 + \beta_1 C_2 + \beta_2 \\ \Delta(3) &= C_3(\alpha_1 C_1 C_2 + \alpha_2 C_2 + \beta_1 C_2 + \beta_2) + \alpha_3 C_3 + \beta_3 \\ &= \alpha_1 C_1 C_2 C_3 + \alpha_2 C_2 C_3 + \alpha_3 C_3 + \beta_1 C_2 C_3 + \beta_2 C_3 + \beta_3 \\ &\dots \\ \Delta(n) &= \alpha_1 p_0 + \alpha_2 p_1 + \dots + \alpha_n p_{n-1} + \beta_1 p_1 + \beta_2 p_2 + \dots + \beta_n p_n \\ &= \alpha_1 p_0 + (\alpha_2 + \beta_1) p_1 + (\alpha_3 + \beta_2) p_2 + \dots + (\alpha_n + \beta_{n-1}) p_{n-1} + \beta_n p_n \\ &= \langle \mathbf{p}, \mathbf{d} \rangle \end{aligned}$$

where  $\mathbf{p} = (p_0, p_1, \dots, p_n)$  and  $\mathbf{d} = (\alpha_1, \alpha_2 + \beta_1, \dots, \alpha_n + \beta_{n-1}, \beta_n)$

In conclusion, the delay difference  $\Delta(n)$  can be represented as the inner product

of the parity vector  $\mathbf{p}$  and the constant vector  $\mathbf{d}$ .

### 5.2.2 Support Vector Machines

Support Vector Machines (SVMs) are powerful learning machines that can perform binary classification of data. Classification is achieved by a linear or nonlinear separating surface in the input space of the dataset. When the feature vectors of the training set are linearly separable by a hyperplane, we can build a linear SVM that uses the structural risk minimization principle to decrease classification errors. The separating surfaces are not necessarily linear. In non-linear SVMs, non-linear functions such as high-order polynomials, radial basis functions, and hyperbolic tangent functions can be exploited to characterize the separating surface.

Here, we give the description of linear SVMs. We consider the problem of classifying  $m$  feature vectors  $\mathbf{x}_1, \dots, \mathbf{x}_m$  in the  $n$ -dimensional real space  $\mathbb{R}^n$ . The goal is to design the hyperplane described by Eqn.

$$g(\mathbf{x}) = \mathbf{w}'\mathbf{x} + w_0 = 0, \quad (5.6)$$

that classifies all dataset correctly. In linear SVMs, we introduce two parallel hyperplanes

$$\mathbf{w}'\mathbf{x} + w_0 = \pm 1$$

to give a margin between two classes of dataset separated by the hyperplane (5.6). Figure 5-2 shows two classes of support vectors and two hyperplanes that divide the entire space into three pieces. To increase the performance of classifiers, the distance between two hyperplanes,  $\frac{2}{\|\mathbf{w}\|}$ , must be maximized. In some cases, the dataset cannot be classified clearly because of non-linearity at the boundary of each class. With respect to this non-linearity, the goal is not only to make the distance as large as possible, but also minimize the number of mis-classifications. Mathematically,

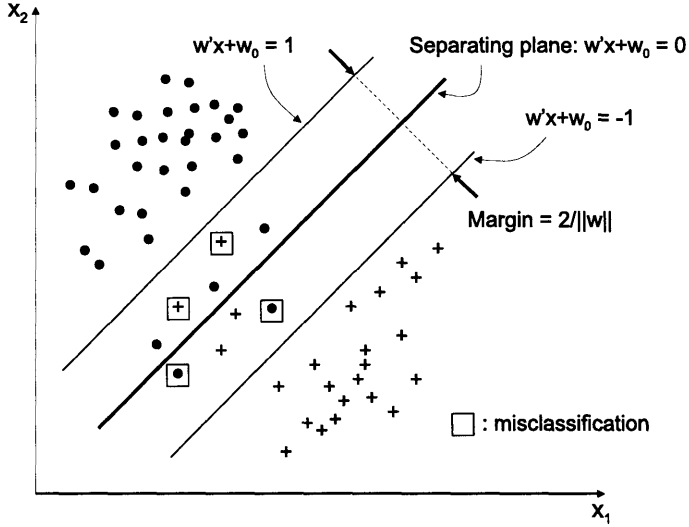


Figure 5-2: The bounding planes with a soft margin and the plane approximately separating classes

this is equivalent to minimizing the cost function

$$J(\mathbf{w}, w_0, n_e) = \frac{1}{2} \|\mathbf{w}\|^2 + \nu n_e,$$

where  $n_e$  is the number of mis-classifications. The parameter  $\nu$  is the positive constant that controls the relative influence of two competing terms. Lagrangian Support Vector Machines (LSVMs) provide a fast converging algorithm to the minimal point of the cost function [14]. Using the linear kernel of a LSVM [15], we can find the hyperplane  $(\mathbf{w}, w_0)$  that minimizes the number of mis-classifications and maximizes the decision margin between two classes.

According to the analysis we did in Section 5.2.1, the arbiter circuit can be viewed as the linear classifier of random challenge vectors in  $n$ -dimensional space, where  $n$  is the number of challenge bits. The parity vectors  $\mathbf{p}$  are the feature vectors and the constant vector  $\mathbf{d}$  is the normal vector of the hyperplane that classifies challenge vectors into two classes. Using the linear SVM, an adversary can build the model of an arbiter-based PUF to predict PUF responses accurately.

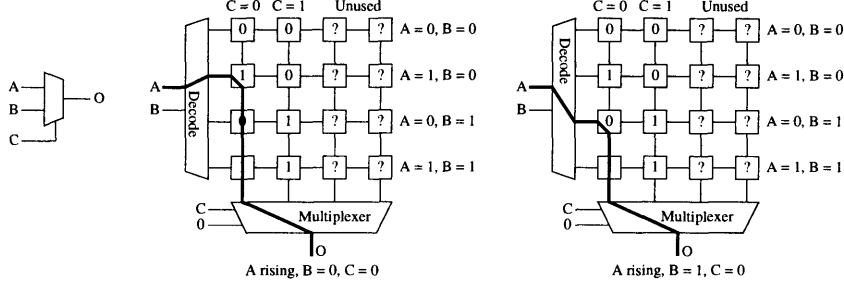


Figure 5-3: The lookup table implementation of a multiplexer in Xilinx FPGAs [2].

## 5.3 Experiments

### 5.3.1 Experiments using a FPGA implementation

To examine how accurate the software model is, we train the machine learning algorithm using 90,000 CRPs measured on a FPGA implementation. When evaluated on a different set of 100,000 challenge-response pairs, the prediction error rate of the model was only about 3.3%. This is greater than the maximum environmental variation (0.3%) and even worse than the inter-chip variation (1.05%) of FPGA implementations. Therefore, the software model can be distinguished from the original PUF by a simple CRP matching.

The experimental results shows that a FPGA implementation of an arbiter-based PUF does not follow our linear additive delay model. Indeed, the switch component in the delay path is implemented by using a pair of multiplexers (MUXs). Each MUX has the challenge bit and both of delay paths as inputs. In Xilinx FPGAs, a combinational logic is mainly implemented using 4 input lookup tables. In particular, in the circuit we implemented, the MUXs are being implemented as lookup tables. These lookup tables are laid out as 4 by 4 grids of SRAM cells as shown in Figure 5-3. As the figure shows, a rising edge that goes through the multiplexer takes a different path through the grid depending on the value of the spectator input that is not currently selected. To take this difference into account would require a more complex model than our first linear model.

To verify the non-linearity of the previous implementation, we synthesized the

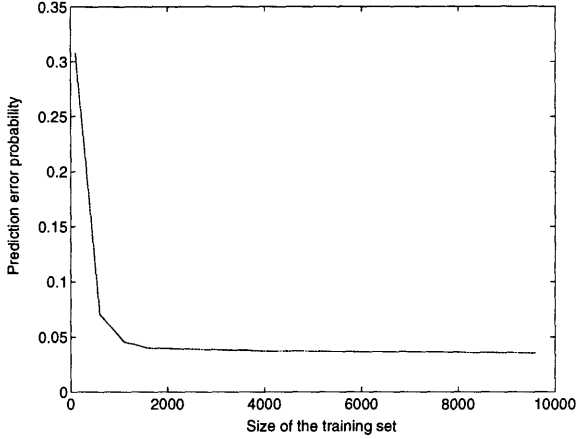


Figure 5-4: The improvement of prediction error rate of the software model according to the size of a training set.

circuit again using the MUXCY component, which is a part of the Xilinx FPGA’s fast carry logic. This component is not implemented in the lookup table and the delay of the MUXCY does not depend on the spectator input. Using the CRPs from this circuit, the prediction error rate of the machine learning algorithm is only 0.61%. Though this result is still above the maximum environmental variation (0.3%) with 40 °C variations in temperature, it is well below inter-chip variation (1.05%). While we cannot conclude that the FPGA implementation of an arbiter-based PUF is broken in a practical range of operation environment, the error rate of prediction is uncomfortably close.

### 5.3.2 Experiments using a Custom Silicon Implementation

Similarly, we evaluate the prediction error rate of a software model using the CRP measured on a custom silicon implementation. We use an SVM to build the software model. In the custom silicon implementation, the structure of delay paths is the same with that of the FPGA implementation. However, the inter-chip variation and environmental variation are different due to technological differences (cf. Section 3.3).

We examine how the prediction error rate changes as a function of the number of training CRPs of the SVM. From a test-chip,  $n$  CRPs are measured to train the

software model. Using the trained model, we predict 100,000 responses of given challenges. We evaluate the prediction error rate of the software model by comparing the predicted responses to actual PUF responses. Figure 5-4 shows the relationship between the size of the training set and the prediction error rate. In this figure, the prediction error rate converges the minimal point (3.55%) when we use more than 5000 training CRPs. The maximum environmental variation of arbiter-based PUFs is 4.82%, which is greater than the prediction error rate of the software model. We conclude that the model can be trained within a trivial amount of time and can impersonate the original PUF successfully.

Consequently, an arbiter-based PUF can be broken by a software modeling attack. There can be two directions of efforts to improve the security of arbiter-based PUFs.

- Adding non-linearity to the PUF circuit to increase the difficulty in modeling building.
- Improving the reliability of PUF responses to lower the environmental variation.

We will discuss the ways of improving the security of arbiter-based PUFs in the next chapter.



# Chapter 6

## Strengthening an Arbiter-Based PUF

The experimental results of software model building show that an arbiter-based PUF is not as secure against model building attacks as we would like. Thus, additional techniques must be developed to improve the security of arbiter-based PUFs. Generally speaking, there are two possible directions to improve the PUF security.

First, adding non-linearity to linear delay paths can improve the security of arbiter-based PUFs. Since the machine learning algorithm exploits the linearity of delay paths, adding non-linearity can make the responses harder to predict by the SVM algorithm and other algorithms. By increasing prediction error probability greater than maximum environmental variation, we can distinguish a software model from an original circuit. To introduce non-linearity in the delay paths, two candidates are proposed: a feed-forward arbiter and a non-linear arbiter. In Section 6.1, we investigate the feasibility and security of new arbiter schemes.

Second, the security of arbiter-based PUFs can be improved by making PUFs more reliable. To impersonate an original PUF with a software model, the prediction error probability must be lower than maximum environmental variation over a practical range. Thus, improving reliability can be helpful to increase the difficulty of software model building. Section 6.2 gives a technique termed a *robust challenge method* that reduces maximum environmental variation of PUF responses.

## 6.1 Secure Delay Models

In the delay paths of arbiter-based PUFs, the delay difference between top and bottom paths is the inner product between a challenge vector and a constant vector. An arbiter works as a linear classifier of the challenge vectors in an  $n$ -dimensional space. In Chapter 5, we have shown that an adversary can build a software model using the machine learning algorithm that estimates the separating hyperplane of challenge vectors to predict PUF responses. The prediction error rate of the software model is less than the maximum environmental variation. The software model can impersonate the original PUF since they are indistinguishable from each other.

To strengthen our PUFs against model building attacks, we propose the non-linear circuit models named *feed-forward arbiters* and *non-linear arbiters*. In both schemes we introduce complex correlation between internal signals to make the delay model non-linear. We have implemented these arbiters in custom silicon and FPGAs, respectively, to verify their viability. From experiments, we evaluate the primary characteristics such as inter-chip variation and environmental variation. Further, we investigate possible model building attacks and examine their prediction accuracies.

### 6.1.1 Feed-forward Arbiter Approach

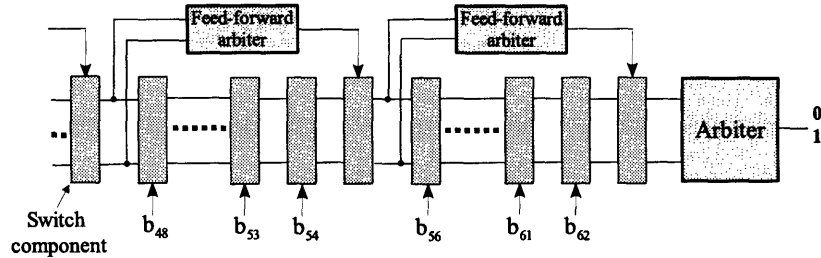


Figure 6-1: Adding unknown challenge bits using feed-forward arbiters (feed-forward arbiter scheme).

One of the non-linear circuit models is a feed-forward arbiter PUF. Figure 6-1 depicts the concept of a feed-forward arbiter PUF scheme. In this scheme, one or

more challenge bits (such as  $b_{55}$  and  $b_{63}$  in the figure) are determined by the result of a race. in intermediate stages instead of being provided by a user.

To build a software model, an adversary must have a sufficient number of CRPs to train the machine learning algorithm. In the feed-forward arbiter circuit, some challenge bits are internally generated and hidden to an adversary. Without probing them, the adversary could make guesses of the hidden bits, but wrong guesses of intermediate challenge bits drop the prediction accuracy significantly. Thus, an adversary needs a more complex software model for predicting the hidden bits to break a feed-forward arbiter PUF.

### Inter-chip variation of feed-forward arbiter PUFs

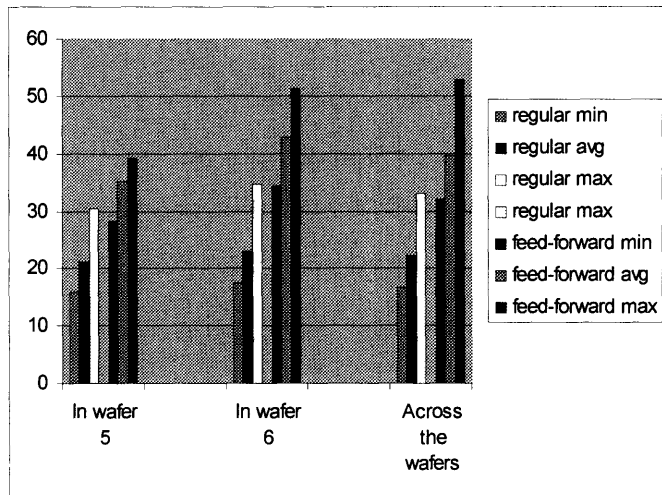


Figure 6-2: Comparison of inter-chip variation between regular arbiter PUFs and feed-forward arbiter PUFs

Figure 6-2 shows the inter-chip variation of feed-forward arbiter PUFs and regular arbiter PUFs. We generated 10,000 CRPs from 5 feed-forward arbiters and evaluated the the inter-chip variation of 10 possible pairs. On average, there exists 38% inter-chip variation between two feed-forward arbiter PUFs. Compared to regular arbiter PUFs, the average inter-chip variation of feed-forward arbiter PUFs is 1.8 times larger than that of regular arbiter PUFs. In the worst case, we still have 28% inter-chip

variation. Inter-chip variation between feed-forward PUFs from the same wafer is similar to the inter-chip variation between the PUFs from different wafers.

In the feed-forward arbiter PUF, there are seven internal arbiters that generate intermediate challenge bits. When there is a difference between at least one of internal arbiter outputs of two PUFs, it is equivalent to evaluating regular arbiter PUFs using different challenges. Since the responses to two different challenges are not equal with 50% probability, the inter-chip variation of feed-forward arbiter PUFs is significantly larger than that of regular arbiter-based PUFs.

Using the delay model in Chapter 4, we model the delay difference of feed-forward PUFs between top and bottom paths for a challenge  $c$  as

$$\Delta_i(c) = \Delta(c) + p_i(c).$$

The distribution of  $\Delta(c)$  in this model is similar to the distribution in regular arbiter PUF because both of them share the same delay paths. From simulation, we verified that  $\Delta(c)$  is Gaussian for random challenges and the standard deviation  $\sigma_\Delta$  of feed-forward arbiter PUFs is similar to that of regular arbiter PUFs. However, the distribution of  $p_i(c)$  is significantly different from regular arbiter PUFs because for feed-forward PUFs,  $p_i(c)$  comes from physical process variation as well as the configuration variation by the inter-chip variation of internal arbiter outputs. Figure 6-3 shows the estimates of  $\sigma_P = \sigma_\Delta/\sigma_p$  for feed-forward PUFs and their accuracy intervals. The estimated  $\sigma_P$  is around 0.6. Assuming that  $\sigma_\Delta$  is similar,  $\sigma_p$  of feed-forward arbiter PUFs is three times larger than that of regular arbiter PUFs.

## **Reliability and Identification Capability**

To be used in practical applications, a feed-forward arbiter PUF must generate consistent responses over a practical range of environment. In the previous section, we studied that the inter-chip variation of internal arbiters in feed-forward arbiter PUFs increases the inter-chip variation of PUF responses significantly. Unfortunately, internal arbiters can also be critical sources of noise. Environmental variation on at

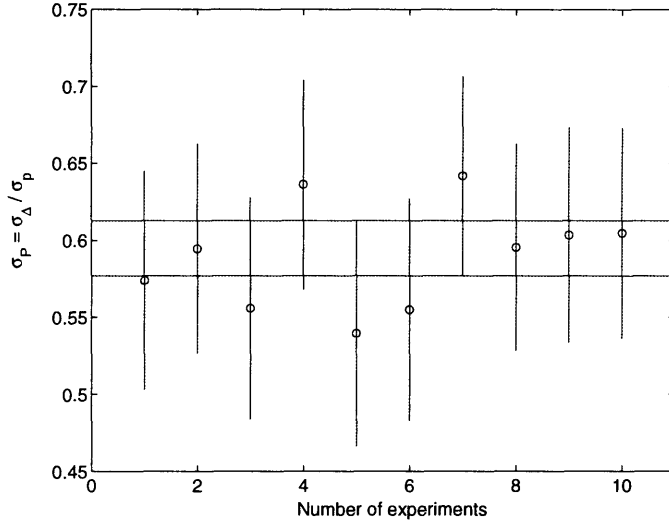


Figure 6-3: Estimates of  $\sigma_P$  and their accuracy intervals for feed-forward arbiter PUFs.

least one of internal arbiter outputs can change the response of a feed-forward arbiter PUF with 50% probability. Since there are seven internal arbiters, feed-forward arbiter PUFs are more likely to be influenced by environmental variation than regular arbiter PUFs.

Figure 6-4 shows the environmental variation of feed-forward arbiter PUFs. Compared to regular arbiter PUFs (cf. Figure 3-7), the maximum environmental variation is 9.84% when temperature changes by 45 °C. That is two times larger than that of regular arbiter PUFs (4.84%). The measurement noise is 4.5%. However, since this environmental variation is still far less than the minimum inter-chip variation (28%), we can identify each feed-forward arbiter PUF even amongst billions of them.

Using the same analysis as in Section 4.4, we can calculate the error probability in identification and authentication of feed-forward arbiter PUFs. We use  $\tau = 0.40$  and  $\mu = 0.10$  as the parameters. When the number of CRPs is 300,  $p_e$  is  $1.6 \cdot 10^{-10}$ , which is less than  $10^{-9}$  (cf Eqn. (4.21)). We had to measure more than 450 CRPs for regular arbiter PUFs to achieve that error probability. Thus, space overhead and performance of identification can be improved by using feed-forward PUFs. When we authenticate feed-forward arbiter PUFs, we need to measure 300 CRPs to obtain

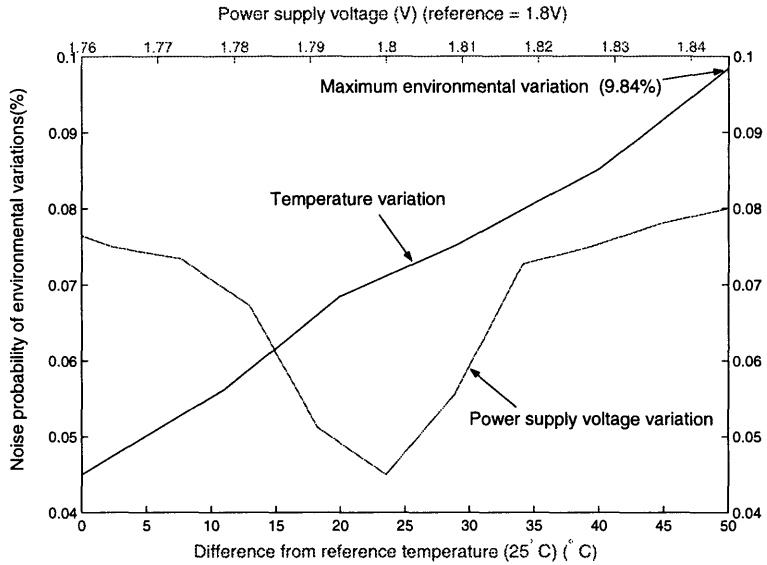


Figure 6-4: Temperature and power supply voltage variations of feed-forward arbiter PUFs.

an error probability of  $7.899 \cdot 10^{-10}$ . This result is better than regular arbiter PUFs, which need 443 CRPs to achieve the same error probability.

### Breaking feed-forward arbiters

Building a software model of feed-forward arbiters is challenging because internal arbiter outputs are hidden to an adversary. Without probing the forward bits, he can no longer exploit the same machine learning algorithms to predict responses. Since the internal arbiters have their own skews which are different from the skew of a final arbiter, he must evaluate more circuit parameters to build a model. Furthermore, the delay difference between top and bottom paths is  $\langle \mathbf{p}, \mathbf{d} \rangle$ , where  $\mathbf{p}$  is not a given challenge vector but a parity vector computed from a challenge vector (cf. Section 5.2.1). Since a bit-flip in the middle of a challenge vector can change half of a parity vector, incorrectly guessing the hidden bits can dramatically lower the prediction accuracy even when the probability of wrong guesses is small.

Here, we present a hybrid method of modeling feed-forward arbiters. Although

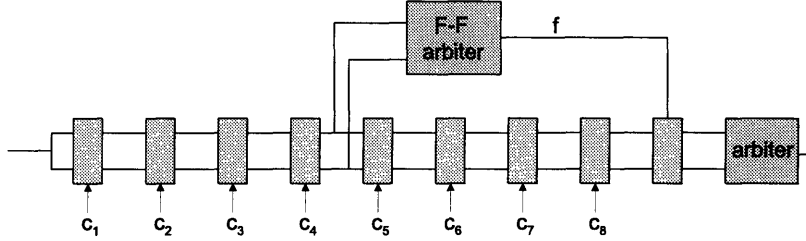


Figure 6-5: The feed-forward arbiter circuit with one feed-forward stage.

predicting the feed-forward arbiter responses is difficult, we can represent a response as a function of challenge bits and circuit parameters. In our implementation, a feed-forward arbiter PUF shares the same delay paths with a regular arbiter PUF. There are seven feed-forward stages and input bits of these stages are multiplexed by a mode bit. In a regular arbiter mode, inputs of these feed-forward stages are connected to external challenge inputs, and in a feed-forward mode, they are connected to internal arbiters' outputs. Thus, the parameters of delay paths except for the skews of internal arbiters can be extracted in the regular arbiter mode by the machine learning algorithm. The adversary can use these delay parameters as supplementary information to complete the software model of feed-forward arbiter PUFs.

We first provide some notation. For a challenge vector  $\mathbf{c} = (c_1, c_2, \dots, c_n)$  where  $c_i \in \{-1, 1\}$ , we denote  $\mathbf{p}(\mathbf{c}) = (p_0, p_1, \dots, p_n)$  as a parity vector of  $\mathbf{c}$  as

$$p_k = \prod_{i=k+1}^n c_i \text{ for } 0 \leq k \leq n-1, p_n = 1.$$

The partial challenge vector  $\mathbf{c}_{i-j} = (c_i, c_{i+1}, \dots, c_j)$  is a part of the challenge vector  $\mathbf{c}$  from the  $i^{\text{th}}$  component to the  $j^{\text{th}}$  component. We denote the concatenation of  $\mathbf{a}$  and  $\mathbf{b}$  by  $\mathbf{a}|\mathbf{b}$ . One-bit output functions  $lb(\mathbf{c})$  and  $rb(\mathbf{c})$  are respectively the leftmost component and the rightmost component of  $\mathbf{c}$ .

Figure 6-5 shows a feed-forward arbiter circuit with one feed-forward stage. When

$\mathbf{c} = (c_1, c_2, \dots, c_8)$  and  $f$  is the output bit of an internal feed-forward arbiter, a response can be expressed by

$$R(\mathbf{c}) = \text{sgn}(\mathbf{p}(\mathbf{c}|f) \cdot \mathbf{d}), \quad (6.1)$$

where  $\text{sgn}(x)$  is a modified sign function as follows.

$$\text{sgn}(x) = \begin{cases} 1 & x \geq 0 \\ -1 & x < 0 \end{cases}.$$

The feed-forward bit  $f$  is

$$f = \text{sgn}(\mathbf{p}(\mathbf{c}_{1-4}) \cdot \mathbf{d}'). \quad (6.2)$$

From the CRPs generated in a regular mode, we can evaluate  $\mathbf{d}$  using a machine learning algorithm. Using the estimated  $\hat{\mathbf{d}}$ , the equation for  $f$  is

$$R(\mathbf{c}) = \text{sgn}\left(f - \frac{rb(\hat{\mathbf{d}})}{\mathbf{p}(\mathbf{c}) \cdot \hat{\mathbf{d}}_{1-9}}\right).$$

From the response and the known parameter  $\hat{\mathbf{d}}$ , we can decide  $f \in \{-1, 1\}$ . Consequently, using Eqn. (6.2), we can estimate  $\mathbf{d}'$  by a machine learning algorithm and complete the predictor function (6.1) with  $\hat{\mathbf{d}}'$ .

Similarly, we can predict outputs of multiple internal arbiters. Figure 6-6 shows a feed-forward arbiter PUFs with two feed-forward stages. The response of this circuit on the challenge  $\mathbf{c}$  can be expressed by

$$R(\mathbf{c}) = \text{sgn}(\mathbf{p}(\mathbf{c}_{1-11} \mid f_1 \mid \mathbf{c}_{12-16} \mid f_2) \cdot \mathbf{d}). \quad (6.3)$$

The internal feed-forward bits  $f_1$  and  $f_2$  can be represented as

$$\begin{aligned} f_1 &= \text{sgn}(\mathbf{p}(\mathbf{c}_{1-6}) \cdot \mathbf{d}') \\ f_2 &= \text{sgn}(\mathbf{p}(\mathbf{c}_{1-11}) \cdot \mathbf{d}''). \end{aligned} \quad (6.4)$$

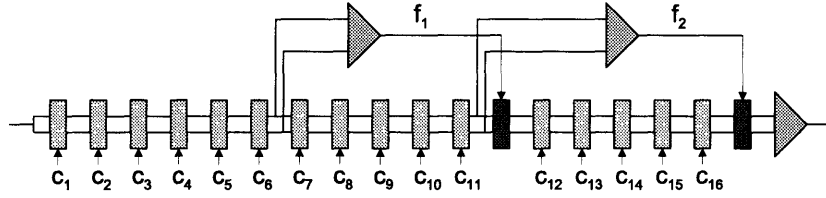


Figure 6-6: The feed-forward arbiter circuit with two feed-forward stages.

By the definition of a parity vector,

$$\begin{aligned}
 & \mathbf{p}(\mathbf{c}_{1-11} \mid f_1 \mid \mathbf{c}_{12-16} \mid f_2) \\
 &= f_2 \mathbf{p}(\mathbf{c}_{1-11} \mid f_1 \mid \mathbf{c}_{12-16}) \mid 1 \\
 &= f_2 lb(\mathbf{p}(\mathbf{c}_{12-16})) \mathbf{p}(\mathbf{c}_{1-11} \mid f_1) \mid f_2 \mathbf{p}(\mathbf{c}_{12-16}) \mid 1 \\
 &= f_2 f_1 lb(\mathbf{p}(\mathbf{c}_{12-16})) \mathbf{p}(\mathbf{c}_{1-11}) \mid f_2 \mathbf{p}(\mathbf{c}_{12-16}) \mid 1
 \end{aligned} \tag{6.5}$$

From Eqn. (6.3), we can represent the response as

$$R(\mathbf{c}) = C_1 f_2 f_1 + C_2 f_2 + C_3,$$

where

$$\begin{aligned}
 C_1 &= lb(\mathbf{p}(\mathbf{c}_{12-16})) \mathbf{p}(\mathbf{c}_{1-11}) \cdot \mathbf{d}_{1-12} \\
 C_2 &= \mathbf{p}(\mathbf{c}_{12-16}) \cdot \mathbf{d}_{13-17} \\
 C_3 &= d_{18}
 \end{aligned}$$

All the constants  $C_1$ ,  $C_2$ , and  $C_3$  can be calculated from challenge bits and the estimated  $\hat{\mathbf{d}}$ .

In this model, we cannot directly decide  $f_1$  and  $f_2$  because we have only the knowledge of one inequality. However, we can infer  $f_1$  and  $f_2$  in the cases below.

- If  $R(\mathbf{c}) = 1$  and  $C_1 f_2 f_1 + C_2 f_2 + C_3$  is positive for only one  $(f_1, f_2)$  among four possible solutions of  $(f_1, f_2)$ , i.e.,  $(1, 1), (1, -1), (-1, 1)$ , and  $(-1, -1)$ , then  $(f_1, f_2)$  can be decided. Similarly, if  $R(\mathbf{c}) = -1$  and  $C_1 f_2 f_1 + C_2 f_2 + C_3$  is negative for only one  $(f_1, f_2)$  among four possible solutions, we can decide  $(f_1, f_2)$ .
- If  $R(\mathbf{c}) = 1$  and  $C_1 f_2 + C_2 f_2 + C_3$  is negative regardless of  $f_2$ , or  $R(\mathbf{c}) = -1$  and  $C_1 f_2 + C_2 f_2 + C_3$  is positive regardless of  $f_2$ , then  $f_1$  must be -1. Similarly, we can decide  $f_1 = 1$  when  $R(\mathbf{c}) = -1$  and  $-C_1 f_2 + C_2 f_2 + C_3$  is positive regardless of  $f_2$ , or  $R(\mathbf{c}) = 1$  and  $-C_1 f_2 + C_2 f_2 + C_3$  is negative regardless of  $f_2$ .
- If  $R(\mathbf{c}) = 1$  and  $C_1 f_1 + C_2 + C_3$  is negative regardless of  $f_1$ , or  $R(\mathbf{c}) = -1$  and  $C_1 f_1 + C_2 + C_3$  is positive regardless of  $f_1$ , then  $f_2$  must be -1. Similarly, we can decide  $f_2 = 1$  when  $R(\mathbf{c}) = 1$  and  $-C_1 f_1 - C_2 + C_3$  is negative regardless of  $f_1$ , or  $R(\mathbf{c}) = -1$  and  $-C_1 f_1 - C_2 + C_3$  is positive regardless of  $f_1$ .

From the simulation with a feed-forward circuit model, for 10,000 measurements of random challenges, more than 4,000  $(f_1, f_2)$  combinations have been uniquely decided. We can estimate the linear classifiers  $\mathbf{d}'$  and  $\mathbf{d}''$  in Eqn. (6.4) with this sufficient amount of  $(\mathbf{p}(\mathbf{c}_{1-6}), f_1)$  and  $(\mathbf{p}(\mathbf{c}_{1-11}), f_2)$  training samples. This method can be generalized to the case when there are  $n$  feed-forward stages.

However, this algorithm is based on the knowledge of a delay vector  $\mathbf{d}$ . If the circuit is hard-wired to the feed-forward mode and  $\mathbf{d}$  cannot be evaluated, then it is still difficult to build a software model of feed-forward arbiter PUFs. On the other hand, since the output of an internal arbiter is in a digital form, the feed-forward arbiter circuit can be vulnerable to physical probing attacks. If we assume that probing a digital signal is viable at every point on an IC, an adversary can build an algorithm to predict internal arbiter outputs. It becomes an equivalent problem to breaking regular arbiter PUFs if the internal arbiter outputs are known to an adversary.

### 6.1.2 Non-linear Arbiter-based PUF Approach

Although feed-forward arbiter PUFs have increased the modeling complexity of our circuit, our circuit is still vulnerable to physical probing attacks because the outputs of internal arbiters are digital. To prevent physical attacks, let us base our design on the premise that any kind of a digital signal that can provide critical information for model building attacks is not revealed to an adversary. As one candidate for possible solutions, we could insert non-linear functions to give a correlation between challenge bits and delay parameters. Figure 6-7 shows a general description of one stage of the whole delay paths. This approach is nice as it leads to continuous delay paths, but is hard to model because of non-linear functions. As non-linear functions,  $\text{MIN}(d_1, d_2)$ , which outputs a minimum delay signal between  $d_1$  and  $d_2$ , or  $\text{MAX}(d_1, d_2)$  can be candidates.

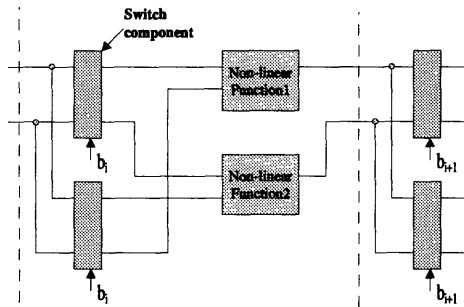


Figure 6-7: A candidate of the non-linear delay paths with non-linear functions.

In experiments, we implement non-linear arbiter PUFs on Xilinx SPARTAN-200S FPGAs using a  $\text{MAX}$  function for the non-linear function 1 and 2. To verify the viability of this non-linear arbiter PUF approach, we evaluate inter-chip variation and environmental variation of non-linear arbiter PUFs. We verify the modeling complexity of non-linear arbiter-PUFs by estimating the amount of non-linearity using the analysis in Chapter 4.

## Feasibility of non-linear arbiter-based PUFs

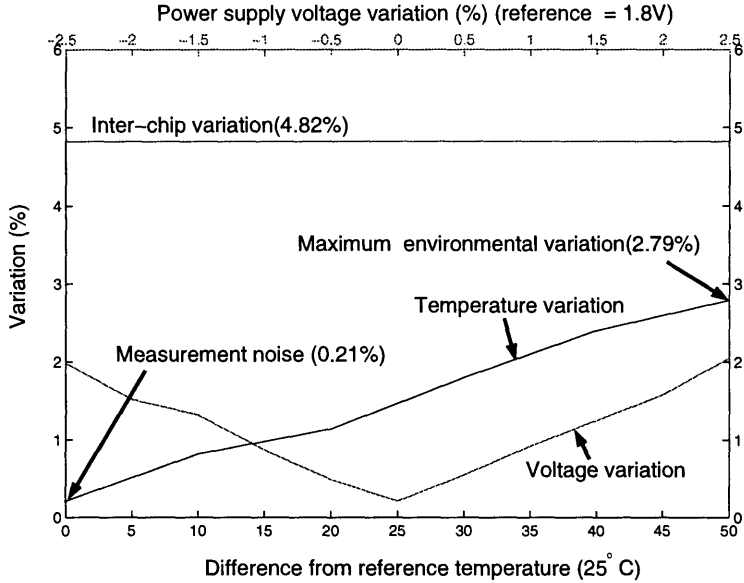


Figure 6-8: Inter-chip variation, temperature variation, and voltage variation of non-linear arbiter PUFs.

Similar to regular arbiter-based PUFs, a non-linear arbiter-based PUF must have sufficient inter-chip variation in order to be identified. In addition, environmental variation of the PUF must be less than the inter-chip variation.

Figure 6-8 shows inter-chip variation and environmental variation of non-linear arbiter PUFs. From 15 PUF pairs, inter-chip variation is 4.82% on average and 3.72% as a minimum. Over a practical range ( $\pm 2.5\%$  voltage variation and less than  $50^{\circ}\text{C}$  temperature variation), environmental variation is less than 2.79%. Using  $\tau = 0.0482$  and  $\mu = 0.0279$ , the error probability of simple identification and authentication of non-linear arbiter-based PUFs can be calculated from Eqn. (4.21) and Eqn. (4.22). However, in these FPGA experiments, the inter-chip variation  $\tau$  is too small to obtain a reasonable identification capability. For example, when we have only two PUFs, we need more than 1,000 CRPs to achieve only less than  $10^{-2}$  error probability.

We could not obtain a sufficient amount of inter-chip variation to identify the PUFs efficiently because of asymmetrically synthesized delay paths. Since we do not have full control of circuit synthesis in FPGAs, there is inevitable asymmetry of delay

paths in the circuit layout. This asymmetry reduces an amount of information-bearing challenges that causes different responses across ICs (cf. Section 3.3). However, the inter-chip variation will increase if the layout of delay paths becomes symmetric in custom silicon. For example, inter-chip variation of regular arbiter-based PUFs was only 1.05% in FPGAs, but it has increased up to 22% in custom silicon. Based on this result, we can expect that the custom silicon implementation of the non-linear arbiter PUFs will have sufficient inter-chip variation to identify a large number of chips in an efficient manner.

### **Modeling complexity of non-linear arbiter-based PUFs**

To evaluate the difficulty in the software model building of non-linear arbiter PUFs, we measure the non-linearity of responses using the non-linear delay model in Chapter 4. Based on the additive delay model (cf. Section 4.1), if estimates of a model parameter cannot be included within an high probability accuracy interval, we must introduce non-linearity in the model to account for experimental results. The required amount of non-linearity provide evidence of modeling complexity of a given PUF structure. For instance, if responses of a PUF follow our linear model and all estimates of a model parameter are within an accuracy interval, then delay differences can be represented as a linear function of random challenges. An adversary can build a polynomial time software model to predict responses based on the linear function. If the responses do not follow the linear model, an adversary needs more effort to build more sophisticated non-linear model to break the PUF.

To compare the non-linearity of the two PUFs, a regular arbiter PUF and non-linear arbiter PUF, Figure 6-9 shows  $p_t - R'_t$  curves of the two PUFs from experimental results. At the dashed line (when  $p_t = 10^{-0.1}$ ), the non-linear arbiter PUFs require 23 times larger non-linearity than regular arbiters to obtain an overlap region between accuracy intervals. From this comparison, we conclude that the model building of a non-linear arbiter PUF is more difficult than that of a regular arbiter PUF.

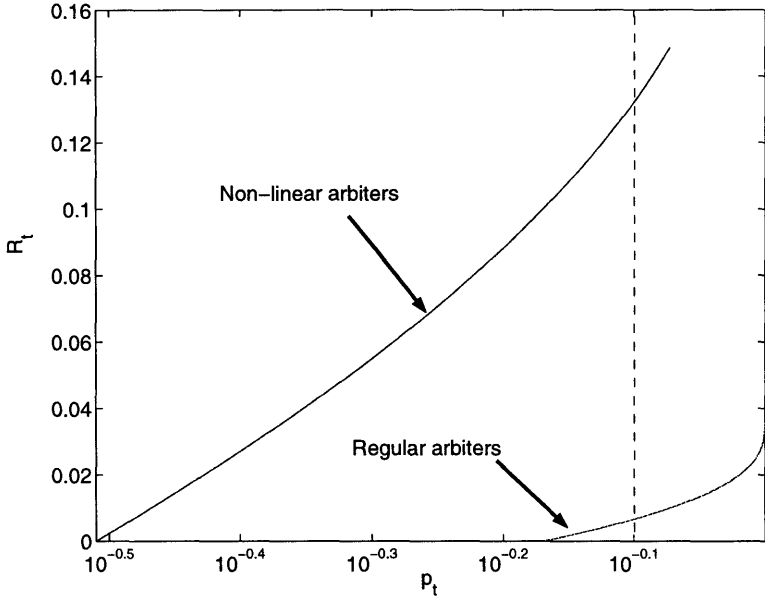


Figure 6-9: Comparison of non-linearity between non-linear arbiter PUFs and regular arbiter PUFs.

## 6.2 Reliability

For an adversary's software model to be successful, the response prediction must have less errors than the maximum environmental variation. Thus, improvement of PUF reliability can increase the difficulty of software model building. We can increase reliability of PUF responses by excluding the challenges that generate inconsistent responses when environmental parameters such as temperature and supply voltage change. However, if some challenges are sensitive to environmental variation, then they are also sensitive to process variation of PUF circuits. Consequently, excluding the unreliable challenges can also reduce inter-chip variation of PUFs, which can decrease identification capability of PUFs. Therefore, we should make careful decisions when excluding unreliable challenges to keep the amount of inter-chip variation sufficiently high.

### 6.2.1 Distribution of Random Challenges

We can model a distribution of random challenges according to the delay difference between top and bottom paths,  $\Delta(c)$ , as Gaussian. Conceptually, we define two range of  $\Delta(c)$ , an environmental variation range and an inter-chip variation range.

- *Environmental variation range:* When  $\Delta(c)$  is within an environmental variation range, the response of a challenge  $c$  is likely to be changed by environmental variation. The differential structure of an arbiter-based PUF helps to reduce the width of this range by rejecting a significant amount of environmental variation.
- *Inter-chip variation range:* When  $\Delta(c)$  is within an inter-chip variation range, the response of the challenge  $c$  is likely to be changed by process variation. Therefore, the challenges within this range can bear the identification information of PUFs.

Figure 6-10 shows the distribution of random challenges and the ranges of environmental variation and inter-chip variation. The shaded part is the range of robust information-bearing challenges which generate identification information of PUFs but are not likely to be affected by environmental variation. In order to improve the reliability, we should exclude the challenges in the environmental variation range to increase the portion of robust information-bearing challenges.

The challenge distribution model of Figure 6-10 can be verified by experiments. From the delay model in Section 5.2.1,  $\Delta(c)$  is proportional to the distance from a challenge vector to the decision hyperplane of a regular arbiter-based PUF model (cf. Chapter 5). Using a machine learning algorithm, the distance from the hyperplane to a challenge vector can be estimated. Consequently, a scaled  $\Delta(c)$  can be calculated for each challenge  $c$  and the distribution of  $\Delta(c)$  can be verified by experimental results.

Figure 6-11 shows the distribution of random challenges according to the distance from the decision hyperplane of an arbiter-based PUF. X-axis of each sub-figure is the distance from the decision hyperplane and Y-axis is the density of challenges. Figure 6-11(a) shows that the distribution of total challenges is Gaussian. In Figure 6-11(b),

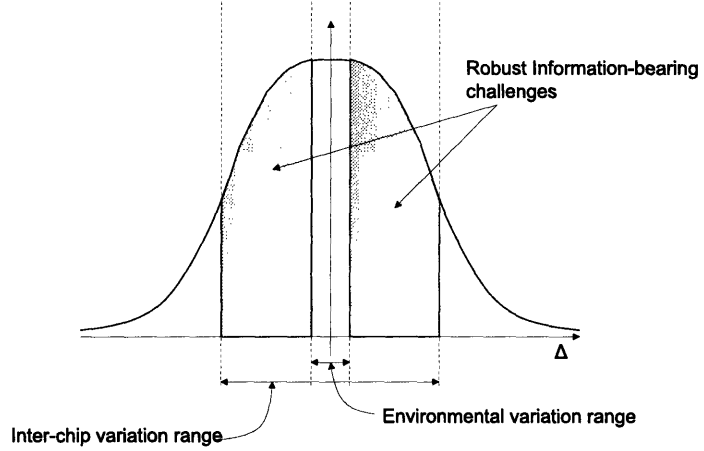


Figure 6-10: Distribution of random challenges according to  $\Delta(c)$

most of the challenges that cause inter-chip variation exist in the interval [0, 0.17]. Compared to the range of this inter-chip variation challenges, from Figure 6-11(c) and 6-11(d), the challenges that cause temperature and voltage variation exist in the narrower interval [0, 0.07]. This result follows our conceptual model of the challenge distribution in Figure 6-10 and verifies the existence of two ranges, an environmental variation range and inter-chip variation range.

### 6.2.2 Robust Challenges

To exclude the challenges that cause unreliable responses, we need an initialization process to test the reliability of a given random challenge. In this process, we examine if the challenge generates consistent responses in repetitive measurements or supply voltage and temperature changes. Practically, without additional expensive cooling, temperature is hard to control within a circuit. Therefore, we use repetitive measurements and supply voltage changes to test the reliability of a given challenge. From these tests, we obtain *robust challenges* that produce consistent responses in controllable environmental changes.

There are several requirements for this method to be useful.

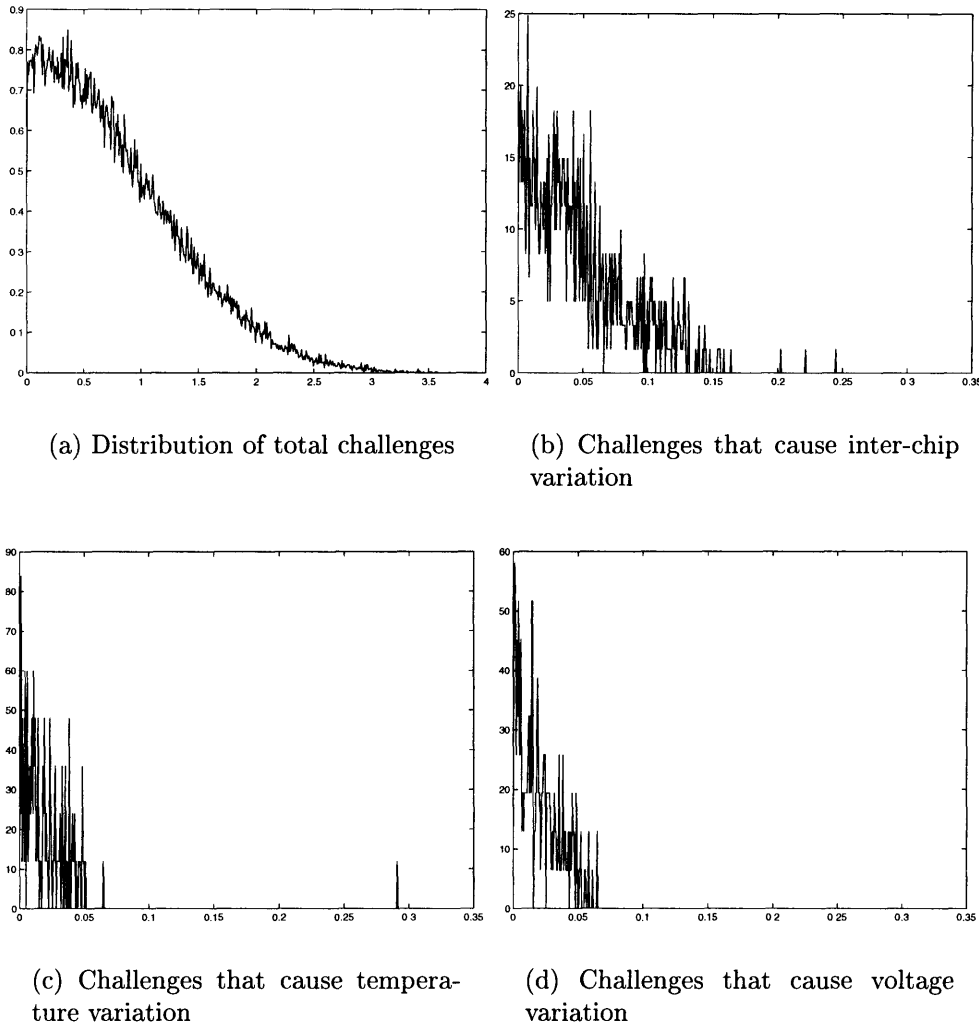


Figure 6-11: Distribution of random challenges according to the distance from the decision hyperplane.

- There must be a sufficient amount of robust challenges in total random challenges.
- Responses from robust challenges must have a reasonable amount of inter-chip variation to identify and authenticate each PUF uniquely.
- The robust challenges should improve the stability against temperature variation.

In experiments, we examine feasibility of the robust challenge method by testing these

requirements.

### Robust challenges to repetitive measurements

To decide the robustness of each challenge, we repeat the same measurement 15 times. When a PUF consistently responds with 0 or 1 to a given challenge for all 15 measurements, the challenge is decided to be robust. Table 6.1 shows inter-chip variation, temperature variation, and voltage variation of regular arbiter-based PUFs using random challenges and robust challenges. From experiments, 83 % of total random challenges are robust in 15 repeated measurements.

	Random challenges	Robust challenges
Inter-chip variation	24.23 %	22.97%
Maximum temperature variation (+45°C)	4.57%	2.54%
Maximum voltage variation ( $\pm 2\%$ )	2.16%	0.19%

Table 6.1: Improvement of reliability using the robust challenges in 15 repetitive measurements.

Using robust challenges costs approximately 1% decrease of inter-chip variation, which can reduce the identification capability of PUFs. However, it gives significant improvements to temperature and voltage variation. The temperature and voltage variation are reduced from 4.57% and 2.16 % to 2.54% and 0.19%, respectively. The reduction of voltage variation comes from the inevitable fluctuation of supply voltage in repetitive measurements.

This reduction of environmental variation is promising because an SVM algorithm can predict responses up to 3.55% error probability. Using robust challenges, we can reduce the maximum environmental variation to 2.54% that is less than prediction error probability. Therefore, an adversary cannot impersonate a PUF circuit with a software model anymore, though we would not advocate using a regular arbiter if one is concerned with software model building attacks.

## Robust challenges to voltage variation

Using an extra circuitry, power supply voltage of a PUF circuit can be automatically controlled; the reliability of a given challenge to voltage variation can be tested by forcing an intentional supply voltage change. In this test, we examine the consistency of responses when  $\pm 1.5\%$  voltage variation is induced. Table 6.2 shows the results of inter-chip variation, temperature variation, and voltage variation of robust challenges against  $\pm 1.5\%$  voltage variation comparing to random challenges. In the entire random challenge set, about 97% of them are robust against the voltage variation. There is less than 1% of inter-chip variation reduction, but using robust challenges improves the reliability of a PUF against temperature and voltage variation from 4.57% and 2.16% to 3.48% and 0.46%, respectively. However, the reduced maximum environmental variation 3.48% is not significantly lower than the prediction error probability of an SVM algorithm.

	Random challenges	Robust challenges
Inter-chip variation	24.23%	23.48%
Maximum temperature variation ( $+45^{\circ}\text{C}$ )	4.57%	3.48%
Maximum voltage variation ( $\pm 2\%$ )	2.16 %	0.46 %

Table 6.2: Improvement of reliability using the robust challenges in  $\pm 1.5\%$  voltage variation.

We can achieve better reliability of responses by using the robust challenges to both repetitive measurements and voltage variation. Let

$$RC_r = \{\text{The robust challenges to 15 repetitive measurements}\}$$

$$RC_v = \{\text{The robust challenges to } \pm 1.5\% \text{ voltage variation}\}.$$

Let

$$RC = RC_r \cap RC_v.$$

We use the challenges in  $RC$  to measure the inter-chip variation and environmental

variation.

Table 6.3 shows experimental results of inter-chip variation, temperature variation, and voltage variation. From the results, 82% of random challenges are included in  $RC$ . Therefore, the size of  $RC$  is sufficiently large to be used in practice. Compared to the robust challenges only to repetitive measurements,  $RC$  improves the temperature variation from 2.54% to 2.43%. In addition, the voltage variation of  $RC$  is 0.05% that is almost negligible. Using  $RC$  costs only 1.5% decrease of inter-chip variation.

	Random challenges	Robust challenges
Inter-chip variation	24.23 %	22.84%
Maximum temperature variation (+45°C)	4.57%	2.43%
Maximum voltage variation ( $\pm 2\%$ )	2.16%	0.05 %

Table 6.3: Improvement of reliability using the robust challenges to repetitive measurements and voltage variation.

We conclude that by using the robust challenges, the maximum environmental variation can be reduced to 2.43% while keeping the inter-chip variation between PUFs over 22%. From an identification capability standpoint, with less than 300 CRPs, we can identify and authenticate billions of PUFs with an error probability less than  $10^{-9}$ . More than 33% of space overhead is reduced compared to the result of using random challenges (cf. Section 4.4). Furthermore, since the SVM in Chapter 5 cannot predict responses with less errors than environmental variation, the software model is distinguishable from the original circuit.

### Calibration of PUFs at different temperatures

The maximum temperature variation can be reduced by using multiple reference temperatures. For a given challenge set  $C$ , we denote the response set of a PUF measured at temperature  $T$  by  $R_T(C)$ . Let

$$d(R_{T_1}(C), R_{T_2}(C))$$

be the distance between two CRP sets generated at temperature  $T_1$  and  $T_2$ . When we set a reference temperature ( $T_{ref}$ ) to 25°C, temperature variation at  $T$  can be represented as

$$d(R_T(C), R_{T_{ref}}(C)).$$

The maximum temperature variation  $\mu_t$  is equal to  $d(R_{T_{MAX}}(C), R_{T_{ref}}(C))$ , where  $T_{MAX}$  denotes the maximum temperature (70°C).

Instead of using one reference temperature, we use two reference CRP sets at different temperatures  $T_1$  and  $T_2$ . When identifying/authenticating a PUF at temperature  $T$ , we calculate two distances

$$\begin{aligned} d_1 &= d(R_T(C), R_{T_1}(C)), \\ d_2 &= d(R_T(C), R_{T_2}(C)), \end{aligned}$$

and use the minimum of  $d_1$  and  $d_2$ ,  $MIN(d_1, d_2)$ , as the distance of the PUF from reference CRP sets.

By using  $MIN(d_1, d_2)$ , the maximum allowed temperature change from reference temperatures is reduced by half over the range from  $T_1$  to  $T_2$ . From the experiments in Section 3.3, the distance  $d(R_{T_1}(C), R_{T_2}(C))$  is roughly proportional to the temperature difference  $|T_1 - T_2|$ . Thus, we can reduce the maximum temperature variation over the range from 25 °C to 70 °C, by setting the reference temperatures to 25 °C and 70 °C. Figure 6-12 shows experimental results of measuring  $MIN(d_1, d_2)$  at different temperatures 25, 34, 57, 65, and 70 °C. The maximum of  $MIN(d_1, d_2)$  is 3.74% at  $T = 57^\circ\text{C}$ , which is lower than the original maximum temperature variation (4.34%). However, since the increase of temperature variation is not linear to the increase of a temperature change, using  $MIN(d_1, d_2)$  does not reduce the maximum temperature variation by half.

We can reduce the maximum temperature variation significantly by increasing the number of reference temperatures. For  $n$  CRP sets generated at reference temperatures from  $T_1$  to  $T_n$ , we calculate  $MIN(d_1, d_2, \dots, d_n)$  for the distance of a PUF from reference CRP sets. Since the maximum allowed temperature change from reference

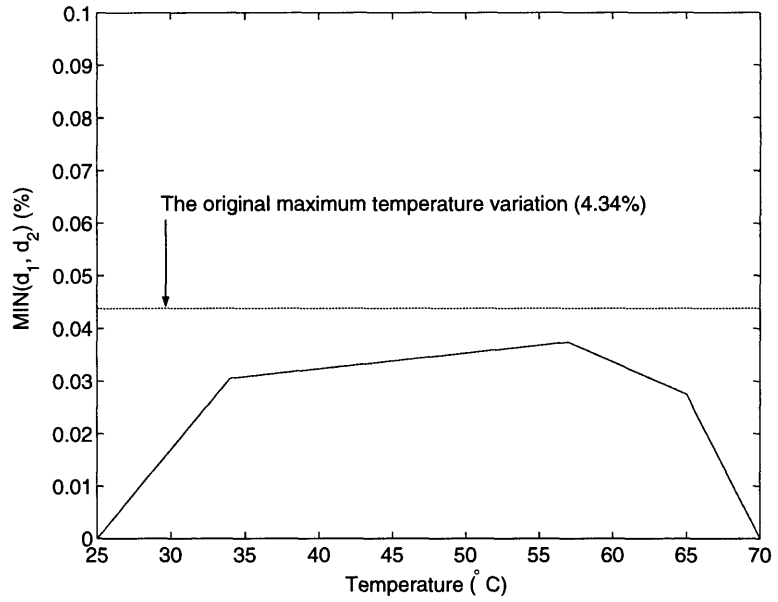


Figure 6-12: Experimental results of  $\text{MIN}(d_1, d_2)$  at different temperature.

temperatures is reduced according to the increase of  $n$ , the maximum temperature variation can be improved. Further, we do not need to assign the reference temperatures linearly. Instead, we can assign reference temperatures more densely around  $T_s$  where  $d(R_T(C), R_{T_{ref}}(C))$  increases more steeply according to the increase of  $T$ . This non-linear assignment of reference temperatures can be helpful to reduce the maximum temperature variation of PUFs.

# Chapter 7

## Conclusion

### 7.1 Ongoing and Future Work

#### 7.1.1 Reliable Secret Sharing with PUFs

Gassend et. al. defined a controlled PUF (CPUF) in [9], which can only be accessed via an algorithm that is physically linked to the PUF in an inseparable way (i.e., any attempt to circumvent the algorithm will lead to the destruction of the PUF). To go beyond the simple authenticated identification applications of PUFs in this thesis, we can use CPUFs to enable secret sharing with a remote user. Through the secret sharing, CPUFs can be used for applications such as trusted third party computation, certified execution and software licensing.

In certified execution, a remote user Alice, who has CRPs, wants to share a secret with the processor with a PUF. To obtain a shared secret, Alice transmits challenges from CRPs in her database to the processor with the PUF. Ideally, the PUF computes corresponding responses. Based on the shared responses, Alice and the processor with the PUF distill a shared secret key.

However, noise is present in PUF responses (cf. Section 3.3). Because of the noise, a practical implementation of a PUF does not immediately lead to a deterministic function. Though we have improved the reliability of PUFs using robust challenges (cf. Section 6.2), noise of 2.43% caused by environmental changes still exists in PUF

responses. To correct the noise, redundant information needs to be transmitted over a public (untrusted) network between Alice and the processor with the PUF. This redundant information must not leak any information about the shared secret key since the redundant information can be used by an adversary Eve (who taps the public network) to reproduce the shared secret key.

In [19], a reliable secret sharing protocol has been suggested to solve the problem of certified execution. In this protocol, Alice encrypts an input of a program with a randomly generated secret key. She also computes redundant information based on the key and PUF responses of a challenge set  $C$  in her database. She transmits to the processor with the PUF the program, the encrypted input, the challenge set  $C$ , and the redundant information. The processor measures (noisy) responses of  $C$  using the PUF and distills the secret key from the responses and the redundant information. Using the secret key, the processor decrypts the encrypted input and executes the program with the input. An output of the execution is encrypted using the secret key and transmitted to Alice.

A mathematical analysis based on fuzzy extractors [7] shows that the noise  $\mu$  caused by the maximum environmental variation on a PUF can be corrected by the redundant information. From calculation, when  $\mu = 4.8\%$ , for example, Alice and a processor with a PUF can reliably share a secret key of 160 bits using 1,800 CRPs in the protocol. A BCH code is used to generate redundant information. When inter-chip variation is 23%, a processor with a different PUF can reproduce the secret key with negligible probability.

An adversary can also learn the redundant information transmitted during the protocol by tapping a public network. If he can predict responses of the PUF with an error rate close to the maximum environmental variation, then he can also reproduce the secret key from the redundant information. To prevent the prediction of responses, we can employ non-linear arbiters such as feed-forward arbiter PUFs and non-linear arbiter PUFs (cf. Section 6.1). It is difficult for an adversary to build an appropriate software model of these arbiters.

### 7.1.2 Reconfigurable PUFs using Non-volatile Storage

To protect the privacy of data in untrusted memories, we encrypt all data using the public key of a trusted processor. The data can only be decrypted using the private key stored in the trusted processor. Unfortunately, the hard-wired private key in the processor is no longer secure against sophisticated physical attacks. For this reason, a PUF can be a good candidate of a private key generator, which is secure against physical attacks.

However, one is also concerned with the integrity of the data stored in untrusted memory. The private key generation by a PUF is vulnerable against replay attacks. Encrypted data stored in a memory can be replaced by other data encrypted correctly with the same private key. The replays of data can cause abnormal operations of the processor and an adversary can exploit the vulnerability of the processor. As a simple solution to the replay attack, a message authentication code (MAC) of each encrypted data block can be used to detect tampering of data. Nevertheless, a replay attack is still possible if an adversary can replay an encrypted data with its MAC together.

In order to prevent the replay attack, we can encrypt each data with different keys. Instead of using static key generation, we generate different public-private key pairs for the encryption and decryption of each data. An adversary cannot replay encrypted data since each of them uses different private keys for decryption. A key generation device must be “reconfigurable” to generate different keys each time we use it.

However, some problems in private key management must be considered. When we store new data, a new public-private key pair must be generated. If old data have not been decrypted yet, the private key of the old data must be stored somewhere in a memory. However, the private key stored in an untrusted memory can be vulnerable to physical attacks. An adversary can even replay encrypted data with the private key together.

Instead of storing private keys in an untrusted memory, we can employ multiple key generation devices in the processor. In the beginning of operation, all the devices

are available. For the encryption of new data, one of available devices is used to generate a new key. This device is not be available until it is used again to generate a private key to decrypt the data. After the decryption, the device is reconfigured and becomes available to generate a new key in the next use.

To realize a reconfigurable PUF, we can exploit a non-volatile storage device to change the delay characteristic of PUFs and preserve the characteristic for a long period. A floating-gate transistor, which is widely used in EPROMs and EEPROMs, can be a good candidate of the non-volatile storage device.

Figure 7-1 shows the concept of a reconfigurable PUF. We can shift the threshold voltage ( $V_{th}$ ) of a floating gate transistor by changing the amount of charge in the floating gate. The shift of  $V_{th}$  changes the transistor delay and the whole delay characteristic of a PUF. Using this property, we can reconfigure the PUF by recharging the floating gate with a different amount of charges. After the reconfiguration, the PUF will respond differently to the same challenges. The PUF will not be changed until the next reconfiguration since the floating gate is effectively non-volatile storage.

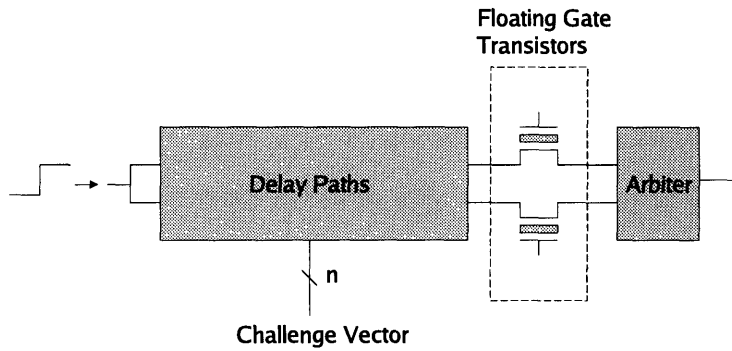


Figure 7-1: The circuit diagram of a reconfigurable arbiter-based PUF.

### 7.1.3 PUF-based Physical Random Number Generators

Random numbers are employed today for most of cryptographic systems. Numerical pseudo-random number generation rely on the computational complexity. However,

*true* random numbers cannot be generated by computational algorithms since the algorithms are deterministic. Instead of using computational algorithms, random physical phenomena can be used to generate true random numbers. Proving the true randomness of physical random number generation is difficult because there can be unknown correlation in generated sequences. Nevertheless, physical random number generation can be useful because equivalent algorithms to simulate and predict the physical phenomenon may not exist.

We can exploit the unreliability of PUF responses to build a physical random number generator. There exists measurement noise which comes from the instability of an arbiter when it is in a racing condition (cf. Section 3.3). Figure 7-2 shows the distribution of the random variable  $k$ , which is the number of 1s in 200 repeated measurements for a given challenge. In the middle of the density function, there exist the challenges whose responses consist of 50% 1s and 50% 0s. Without environmental variation, the responses of these challenges are likely to be random in repeated measurements.

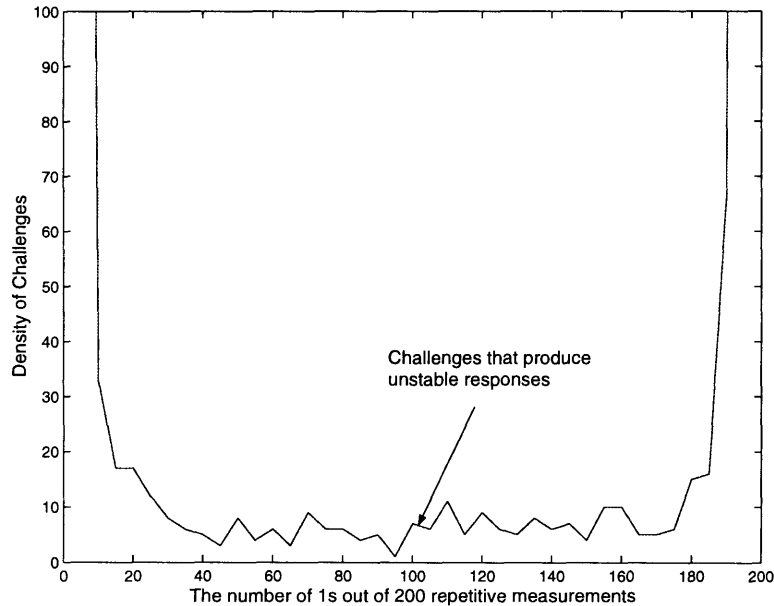


Figure 7-2: The density function of the random variable  $k$ , where  $k$  is the number of 1s out of 200 repetitive measurements.

In fact, the unreliability of PUF responses depends on an environmental condition such as temperature and power supply voltage. One challenge that generates reliable responses in one condition can generate unreliable responses in another. Thus, each time we use a PUF to generate random bits, we must test responses of a number of random challenges to find the challenges that generate random responses. Statistically, from 10,000 random challenges, there exist approximately 10 challenges whose responses are random. Based on the performance of the PUF circuit (cf. Section 3.3), it takes 0.5 sec to test the randomness of 10,000 challenges by 1,000 repeated measurements. This initialization of a PUF-based random number generator can be completed within 1 sec.

Compared to other physical random number generators, the PUF-based random number generator can be a compact and low-power solution. A 64-stage PUF circuit costs only less than 1000 gates and the circuit can be implemented using a standard IC manufacturing process. Additionally, various kinds of low power techniques such as sub-threshold logic design and multi-thresholds CMOS design can be utilized to reduce the power consumption of the PUF circuit. The power consumption of the PUF-based random number generator and the quality of random numbers will be examined in future experiments.

# Appendix A

## Parameter Estimation

Let  $c$  be the input to an experiment and let  $R(c)$  be its output. Suppose that we have a statistical model of the experiment using parameters  $x_i$ ,  $1 \leq i \leq k$ . We choose some set  $\mathcal{F}$  for which we can compute<sup>1</sup>

$$\text{Prob}(R(c) \in \mathcal{F}) = F(x_1, \dots, x_k)$$

as a function of the parameters which define our statistical model. We assume that  $F$  is a continuous and a differentiable function. We introduce the notation  $F_i(x_1, \dots, x_l)$  such that

$$F_i(x_1, \dots, x_k) = \frac{\partial}{\partial x_i} F(x_1, \dots, x_k)$$

**Theorem A.1** Suppose that, for  $1 \leq i \leq k - 1$ ,  $E_i$  is an estimate for  $x_i$  such that

$$|x_i - E_i| \leq \varepsilon_i$$

with probability at least  $1 - p_i$ .

Let  $\mathcal{C}$  be an arbitrary set of inputs, let

$$E = \frac{|\{c \in \mathcal{C} : R(c) \in \mathcal{F}\}|}{|\mathcal{C}|},$$

---

<sup>1</sup>The probability is taken over a uniform distribution of inputs  $c$ .

and define  $E_k$  as the solution of

$$E = F(E_1, \dots, E_{k-1}, E_k)$$

(we suppose that it exists).

Let  $\varepsilon > 0$  and

$$p = 2Q(-2\varepsilon\sqrt{|\mathcal{C}|}).$$

Define

$$p_k = 1 - (1-p) \cdot \prod_{i=1}^{k-1} (1-p_i).$$

There exist  $\theta_i \in [0, 1]$ ,  $1 \leq i \leq k$ , such that

$$F(x_1, \dots, x_k) - E = \sum_{i=1}^k (x_i - E_i) F_i(z_1, \dots, z_k), \quad (\text{A.1})$$

where

$$z_i = \theta_i x_i + (1 - \theta_i) E_i.$$

Suppose that  $F_k(z_1, \dots, z_k) \neq 0$  and let

$$\varepsilon_k = \left( \varepsilon + \sum_{i=1}^{k-1} |F_i(z_1, \dots, z_k)| \varepsilon_i \right) \frac{1}{|F_k(z_1, \dots, z_k)|}.$$

Then

$$|x_k - E_k| \leq \varepsilon_k$$

with probability at least  $1 - p_k$ .

We call  $|x_i - E_i| \leq \varepsilon_i$  an *accuracy intervals* for  $x_i$ . If  $\varepsilon_i$  is small enough, then

$$F_i(z_1, \dots, z_k) \approx F_i(E_1, \dots, E_k).$$

If this approximation holds for  $1 \leq i \leq k$ , then we can apply the theorem to compute an accuracy interval for  $x_k$ .

We can also use second derivatives of  $F$  and show that there are no local minima or

local maxima in the region defined by the  $k$  accuracy intervals. Then  $F_i^\leftarrow(z_1, \dots, z_k)$  can be lower and upper bounded by boundary points of the region. These bounds can be used to compute an accuracy interval for  $x_k$ .

Notice that if  $F_k(z_1, \dots, z_k) = 0$  then function  $F$  does not depend on the  $k^{\text{th}}$  variable in a neighborhood of  $(z_1, \dots, z_k)$ . In particular, the value of  $F(x_1, \dots, x_k)$  does not depend on  $x_k$ . This shows that  $\mathcal{F}$  cannot be used to accurately estimate  $x_k$ .

*Proof.*

By the law of large numbers, the binomial distribution that defines  $E$  tends to a normal distribution

$$N(E, \sqrt{E(1-E)/|\mathcal{C}|}).$$

(notice that  $E(1-E) \leq 1/4$ ). This proves that,

$$\begin{aligned} \text{Prob}(|E - F(x_1, \dots, x_k)| \geq \varepsilon) &\approx 2 \int_{t=-\infty}^{-\frac{\varepsilon\sqrt{|\mathcal{C}|}}{\sqrt{E(1-E)}}} \frac{e^{-t^2/2}}{\sqrt{2\pi}} dt \\ &\leq 2 \int_{t=-\infty}^{-2\varepsilon\sqrt{|\mathcal{C}|}} \frac{e^{-t^2/2}}{\sqrt{2\pi}} dt 2Q(-2\varepsilon\sqrt{|\mathcal{C}|}) = p. \end{aligned} \quad (\text{A.2})$$

From (A.1) we infer that

$$\begin{aligned} |(x_k - E_k)F_i(z_1, \dots, z_k)| &= |(E - F(x_1, \dots, x_k)) - \sum_{i=1}^{k-1} (x_i - E_i)F_i(z_1, \dots, z_k)| \\ &\leq |E - F(x_1, \dots, x_k)| + \sum_{i=1}^{k-1} |x_i - E_i| \cdot |F_i(z_1, \dots, z_k)| \\ &\leq |E - F(x_1, \dots, x_k)| + \sum_{i=1}^{k-1} \varepsilon_i \cdot |F_i(z_1, \dots, z_k)| \end{aligned}$$

holds with probability at least

$$P = \prod_{i=1}^{k-1} (1 - p_i).$$

Additionally,

$$|E - F(x_1, \dots, x_k)| \leq \varepsilon$$

holds with probability at least  $1 - p$ . Therefore,

$$\text{Prob}(|x_k - E_k| \leq \varepsilon_k) \geq (1 - p) \prod_{i=1}^{k-1} (1 - p_i).$$

Consequently, the error probability  $\text{Prob}(|x_k - E_k| > \varepsilon_k)$  is at most  $p_k$ .

Independent experiments, represented by different sets  $\mathcal{F}$  and functions  $F$ , lead to different estimates. Only if the different estimates fall within one another's accuracy intervals, we believe the statistical model. This shows how the theorem can be used to verify our statistical model.

## Appendix B

### Properties of $Q(x)$

Let

$$\begin{aligned}
Q(x) &= \int_{t=-\infty}^x \frac{e^{-t^2/2}}{\sqrt{2\pi}} dt \\
&= \frac{1}{2} + \int_{t=0}^x \frac{e^{-t^2/2}}{\sqrt{2\pi}} dt \\
&= \frac{1}{2} + \frac{1}{\sqrt{2\pi}} \int_{t=0}^x \sum_{k=0}^{\infty} (-t^2/2)^k / k! dt \\
&= \frac{1}{2} + \frac{1}{\sqrt{2\pi}} \sum_{k=0}^{\infty} \int_{t=0}^x (-t^2/2)^k / k! dt \\
&= \frac{1}{2} + \frac{1}{\sqrt{2\pi}} \sum_{k=0}^{\infty} (-1/2)^k \frac{x^{2k+1}}{(2k+1)k!} \\
&= \frac{1}{2} + x - \frac{1}{6}x^3 + \frac{1}{40}x^5 - o(x^7).
\end{aligned}$$

For  $x < 0$ ,

$$(1 - 1/x^2) \frac{e^{-x^2/2}}{\sqrt{2\pi} \cdot x} < Q(x) < \frac{e^{-x^2/2}}{\sqrt{2\pi} \cdot x}. \quad (\text{B.1})$$

The first derivative of  $Q^{-1}(y)$  is equal to

$$\frac{d}{dy} Q^{-1}(y) = \left\{ \frac{d}{dx} Q(x) \Big|_{x=Q^{-1}(y)} \right\}^{-1} = \left\{ \frac{e^{-Q^{-1}(y)^2/2}}{\sqrt{2\pi}} \right\}^{-1} = \sqrt{2\pi} e^{Q^{-1}(y)^2/2}.$$

The second derivative of  $Q^{-1}(y)$  is equal to

$$\frac{d}{dy} \sqrt{2\pi} e^{Q^{-1}(y)^2/2} = 2\pi Q^{-1}(y) e^{Q^{-1}(y)^2},$$

the third derivative of  $Q^{-1}(y)$  is equal to

$$\frac{d}{dy} 2\pi Q^{-1}(y) e^{Q^{-1}(y)^2} = (2\pi)^{3/2} e^{3Q^{-1}(y)^2/2} (1 + 2Q^{-1}(y)^2),$$

and the fourth derivative is equal to

$$\frac{d}{dy} (2\pi)^{3/2} e^{3Q^{-1}(y)^2/2} (1 + 2Q^{-1}(y)^2) = (2\pi)^2 e^{2Q^{-1}(y)^2} (1 + 2Q^{-1}(y)^2) 7Q^{-1}(y)^2.$$

Notice that  $Q^{-1}(1/2) = 0$ , hence,

$$Q^{-1}(1/2 + \varepsilon) = (2\pi)^{1/2} \varepsilon + (2\pi)^{3/2} \varepsilon^3 / 6 + o(\varepsilon^5). \quad (\text{B.2})$$

The second derivative is positive if and only if  $Q^{-1}(y) > 0$ . Hence, by using the first derivative,

$$\left| \frac{Q^{-1}(y) - Q^{-1}(y')}{y - y'} \right| \leq \max\{\sqrt{2\pi} e^{Q^{-1}(y)^2/2}, \sqrt{2\pi} e^{Q^{-1}(y')^2/2}\}. \quad (\text{B.3})$$

Suppose that  $|y - y'| \leq \varepsilon$ . Then (B.3) implies

$$|Q^{-1}(y) - Q^{-1}(y')| \leq \varepsilon \max\{\sqrt{2\pi} e^{Q^{-1}(y)^2/2}, \sqrt{2\pi} e^{Q^{-1}(y')^2/2}\}.$$

If  $y \geq \varepsilon$ , then  $y - \varepsilon \leq y' \leq y + \varepsilon$ . Hence, the maximum in (B.3) is upper bounded by

$$\max\{\sqrt{2\pi} e^{Q^{-1}(y+\varepsilon)^2/2}, \sqrt{2\pi} e^{Q^{-1}(y-\varepsilon)^2/2}\}.$$

We denote this maximum by  $\sqrt{2\pi} e^{Q^{-1}(y \pm \varepsilon)^2/2}$  and we obtain the inequality

$$|Q^{-1}(y) - Q^{-1}(y')| \leq \delta = \sqrt{2\pi} \varepsilon e^{Q^{-1}(y \pm \varepsilon)^2/2}.$$

Concluding, if  $y \geq \varepsilon$  then

$$Prob(|Q^{-1}(y) - Q^{-1}(y')| \geq \delta) \leq Prob(|y - y'| \geq \varepsilon). \quad (\text{B.4})$$



# Bibliography

- [1] A.Bassi, A.Veggetti, L.Croce, and A.Bogliolo. Measuring the effects of process variations on circuit performance by means of digitally-controllable ring oscillators. In *Proceedings of the International Conference on Microelectronic Test Structures(ICMTS)*, 2003.
- [2] B. Gassend, D. Lim, D. Clarke, M. van Dijk, and S. Devadas. Identification and Authentication of Integrated Circuits. *Concurrency and Computation: Practice and Experience*, 2003.
- [3] D. S. Boning and S. Nassif. Models of Process Variations in Device and Interconnect. In A. Chandrakasan, W. Bowhill, and F. Fox, editors, *Design of High Performance Microprocessor Circuits*, chapter 6. IEEE Press, 2000.
- [4] A. Chandrakasan, W. Bowhill, and F. Fox. *Design of High Performance Microprocessor Circuits*. IEEE press, 2000.
- [5] David Chinnery and Kurt Keutzer. *Closing the Gap Between ASIC & Custom*. Kulwer Academic Publishers, 2002.
- [6] Florentin Dartu and Lawrence T. Pileggi. Calculating worst-case gate delays due to dominant capacitance coupling. In *Proceedings of the 34th annual conference on Design automation conference*, pages 46–51. ACM Press, 1997.
- [7] Y. Dodis, L. Reyzin, and A. Smith. Fuzzy extractors: how to generate strong keys from biometrics and other noisy data. In *Advances in Cryptology - Eurocrypt 2004*, 2004.

- [8] Blaise Gassend. Physical Random Functions. Master's thesis, Massachusetts Institute of Technology, January 2003.
- [9] Blaise Gassend, Dwaine Clarke, Marten van Dijk, and Srinivas Devadas. Controlled physical random functions. In *Proceedings of 18<sup>th</sup> Annual Computer Security Applications Conference*, December 2002.
- [10] Oded Goldreich, Shafi Goldwasser, and Silvio Micali. On the Cryptographic Applications of Random Functions . In *Proceedings of Crypto 84 on Advanceds in cryptology*, pages 276–288, 1985.
- [11] Oded Goldreich, Shafi Goldwasser, and Silvio Micali. How to Construct Random Functions. *Journal of the Association for Computing Machinery*, 33:792–807, 1986.
- [12] Paul Kocher, Joshua Jaffe, and Benjamin Jun. Differential Power Analysis. *Lecture Notes in Computer Science*, 1666:388–397, 1999.
- [13] Oliver Kommerling and Markus G. Kuhn. Design principles for tamper-resistant smartcard processors. In *USENIX Workshop on Smartcard Techonlogy*, 1999.
- [14] O. L. Mangasarian and David R. Musicant. Lagrangian support vector machine classification. Technical Report 00-06, Data Mining Institute, Computer Sciences Department, University of Wisconsin, Madison, Wisconsin, June 2000. <ftp://ftp.cs.wisc.edu/pub/dmi/tech-reports/00-06.ps>.
- [15] O.L. Mangasarian and D. R. Musicant. LSVM Software: active set support vector machine classification software, 2000. [www.cs.wisc.edu/~musicant/lsvm/](http://www.cs.wisc.edu/~musicant/lsvm/).
- [16] James A. Power, Brian Donnellan, Alan Mathewson, and William A. Lane. Relating statistical MOSFET model parameter variabilities to IC manufactuing process fluctuations enabling realistic worst case design. *IEEE Trans. on Semiconductor Manufacturing*, 7(3), 1994.

- [17] Jean-Jacques Quisquater and David Samyde. ElectroMagnetic Analysis (EMA): Measures and Counter-Measures for Smart Cards. In *Proceedings of Smart Card Programming and Security (E-smart 2001)*, LNCS 2140, pages 200–210, September 2001.
- [18] P. S. Ravikanth. *Physical One-Way Functions*. PhD thesis, Massachusetts Institute of Technology, 2001.
- [19] Marten van Dijk, Daihyun Lim, and Srinivas Devadas. Reliable secret sharing with physical random functions. Technical report, MIT Computation Structures Group MEMO-475, May 2004. <http://csg.lcs.mit.edu/pubs/>.
- [20] N. Weste and K. Eshraghian. *Principles of CMOS VLSI Design: A Systems Perspective*. Addison Wesley, 1985.